UCSF
UC San Francisco Electronic Theses and Dissertations

Title

Novel E3 Ubiquitin Ligase Regulators of Parkinson's Protein LRRK2

Permalink

https://escholarship.org/uc/item/63s1s36n

Author

Stormo, Adrienne

Publication Date

2020

Peer reviewed|Thesis/dissertation

Novel E3 Ubiquitin Ligase Regulators of Parkinson's Protein LRRK2

by
Adrienne Stormo

DISSERTATION
Submitted in partial satisfaction of the requirements for degree of
DOCTOR OF PHILOSOPHY

in

Biomedical Sciences

in the

GRADUATE DIVISION
of the
UNIVERSITY OF CALIFORNIA, SAN FRANCISCO

Approved:

Committee Members

ACKNOWLEDGEMENTS

Novel E3 Ubiquitin Ligase Regulators of Parkinson's Protein LRRK2

Adrienne Stormo

ABSTRACT

Parkinson's Disease (PD) is a neurodegenerative movement disorder affecting approximately 1% of the population over 60, with no existing treatments that slow, stop, prevent, or reverse neuron loss. Missense mutations in Leucine-Rich Repeat Kinase 2 (LRRK2) are the most common identified cause of PD; however, the disease-driving and normal cellular functions of LRRK2 are not fully defined. We used two screening approaches to gain insight into LRRK2 function and regulation: a proteomic screen to identify novel LRRK2 interactors, and a CRISPRi screen to identify modifiers of LRRK2 turnover. Our proteomic screen generated a quantitative global interactome of full-length LRRK2 that identified 48 novel interacting proteins, including Tripartite Motif-Containing Protein 1 (TRIM1), a microtubule-associated E3 ubiquitin ligase. We find that TRIM1 binds an unstructured regulatory domain on LRRK2 to recruit it to the microtubule. Furthermore, TRIM1 ubiquitinates LRRK2, leading to its proteasomal degradation. Expression of TRIM1 also modulates LRRK2 kinase activity and cytotoxicity: TRIM1 inhibits Rab29-mediated LRRK2 kinase activation and rescues the neurite outgrowth deficit caused by the most common PD-driving mutation, LRRK2 G2019S. In our second screen, we sought to identify additional novel regulators of LRRK2 turnover, focusing on proteasomal degradation caused by pharmacological LRRK2 kinase inhibition. LRRK2 kinase inhibitors are a promising therapeutic strategy for PD, but also lead to ubiquitination and degradation of LRRK2 by

unknown ubiquitin ligases, which appears to cause pulmonary toxicity in non-human primates. We identified two additional E3 ubiquitin ligases that target LRRK2 for degradation downstream of kinase inhibition. Together, these findings identify LRRK2 localization, ubiquitination, and degradation as important regulatory events with relevance for kinase activity, cytotoxicity, and pharmacological intervention in PD.

TABLE OF CONTENTS

LIST OF FIGURES

LIST OF TABLES

CHAPTER I: INTRODUCTION

Parkinson's Disease

Prevalence

Parkinson's Disease (PD) is the second most common neurodegenerative disease, behind Alzheimer's Disease [1]. It affects approximately 1% of the population over 60 years of age, and 5% of those over 80 [2]. On the whole, nearly 1 million people in the United States have been diagnosed with PD [3], and there are undoubtedly many more in the early stages of disease who have not yet been diagnosed. A recent report estimated that PD in the United States costs over 25 billion dollars in direct medical costs, and an additional 26 billion dollars in indirect costs, such as lost earnings from patients who can no longer work or family members who are needed for intensive full- or part-time care [4]. Furthermore, as the population ages, the number of affected people and the economic burden of PD are only likely to grow. PD is already a substantial medical concern in the United States and worldwide, and developing effective therapies is an essential goal.

Symptoms

PD is a neurodegenerative movement disorder, which means that it is characterized by a progressive loss of neurons and classically causes movement-related symptoms. The hallmark symptoms include bradykinesia (slowness of movement and difficulty starting motions), a resting tremor, rigidity, and balance impairment [5]. Patients can also present with non-movement symptoms, like depression, sleep disruption, and/or dementia [5]. On a cellular level, PD is defined by a loss of dopaminergic neurons in the substantia nigra pars compacta in the

midbrain [6].   Normally, dopaminergic neurons synthesize and release dopamine, a neurotransmitter, which is essential for movement control via the nigrostriatal pathway [7], and thus loss of these neurons leads to the symptoms associated with PD. Additionally, PD is often, but not always, pathologically marked by the presence of Lewy bodies [5]. Lewy bodies are protein aggregates consisting primarily of α-synuclein, ubiquitin, and sometimes other insoluble proteins [8]. Unfortunately, PD progresses silently for a long time – symptoms don't present until roughly 60-80% of the nigral neurons are gone [1], meaning by the time patients are diagnosed, they are already in an advanced stage of the disease.   While there are some symptomatic treatments available, there are currently no treatments that prevent, stop, or reverse neuron loss [9].

Genetics

Understanding the etiology of PD is an important step towards developing new treatments; however, underlying disease mechanisms have been hard to interrogate. The vast majority of PD cases are sporadic, with rare cases linked to environmental causes, such as 1-methyl-4-phenyl-1,2,3,6-tetrahydropyridine (MPTP)-induced PD [10]. However, about 10% of PD cases are familial, with a handful of genes identified as definitively causal [6] (Figure 1.1A). Mutations in six genes inarguably lead to PD in a Mendelian fashion: SNCA, Parkin, PINK1, DJ-1, LRRK2, and VPS35 (Figure 1.1B). Briefly, SNCA, which encodes α-synuclein, a protein found in presynaptic terminals, was the first gene in which mutations were definitively linked to PD [11]. SNCA mutations lead to early-onset PD (i.e. diagnosis before the age of 50) in an autosomal dominant fashion. Parkin is an E3 ubiquitin ligase; mutations in this gene lead to autosomal recessive, early-onset PD [12]. Parkin mutations are the most common in familiar

2

PD, and cause a majority of the (rare) familial PD cases in people under 30 [6]. PTEN-Induced Kinase 1 (PINK1) is a mitochondrial kinase, and is thought to act in the same pathway as Parkin, as an upstream activator [6]. Like Parkin, PINK1 mutations cause early-onset PD in an autosomal recessive manner [13]. DJ-1 is less understood, but is also thought to be important for the maintenance of mitochondria, along with PINK1 and Parkin [14]. Like those genes, autosomal recessive mutations in DJ-1 also cause early-onset PD [15].

On the other hand, mutations in Leucine-Rich Repeat Kinase 2 (LRRK2) and Vacuolar Protein Sorting-associated protein 35 (VPS35) both cause typical-onset PD (affecting people over the age of 50), both in an autosomal dominant fashion [16-19]. VPS35 is a component of the retromer complex and is involved in endosomal trafficking [6]. Mutations in VPS35 are extremely rare, but mutations in LRRK2 are among the most common in familial PD. Additionally, LRRK2 mutations are found in 1-3% of sporadic PD cases [1]. Between familiar and sporadic cases, LRRK2 mutations are the most common identified cause of PD [20]. Beyond these six genes, there are still some unidentified PD loci, as well as some genes that have lower penetrance but contribute some to PD risk (Table 1.1). Finally, there are also common variants identified through genome-wide association studies (GWAS) that contribute small increases in PD-associated risk [6, 21] (Figure 1.1B). Notably, different mutations in LRRK2 fall into all three of these categories.
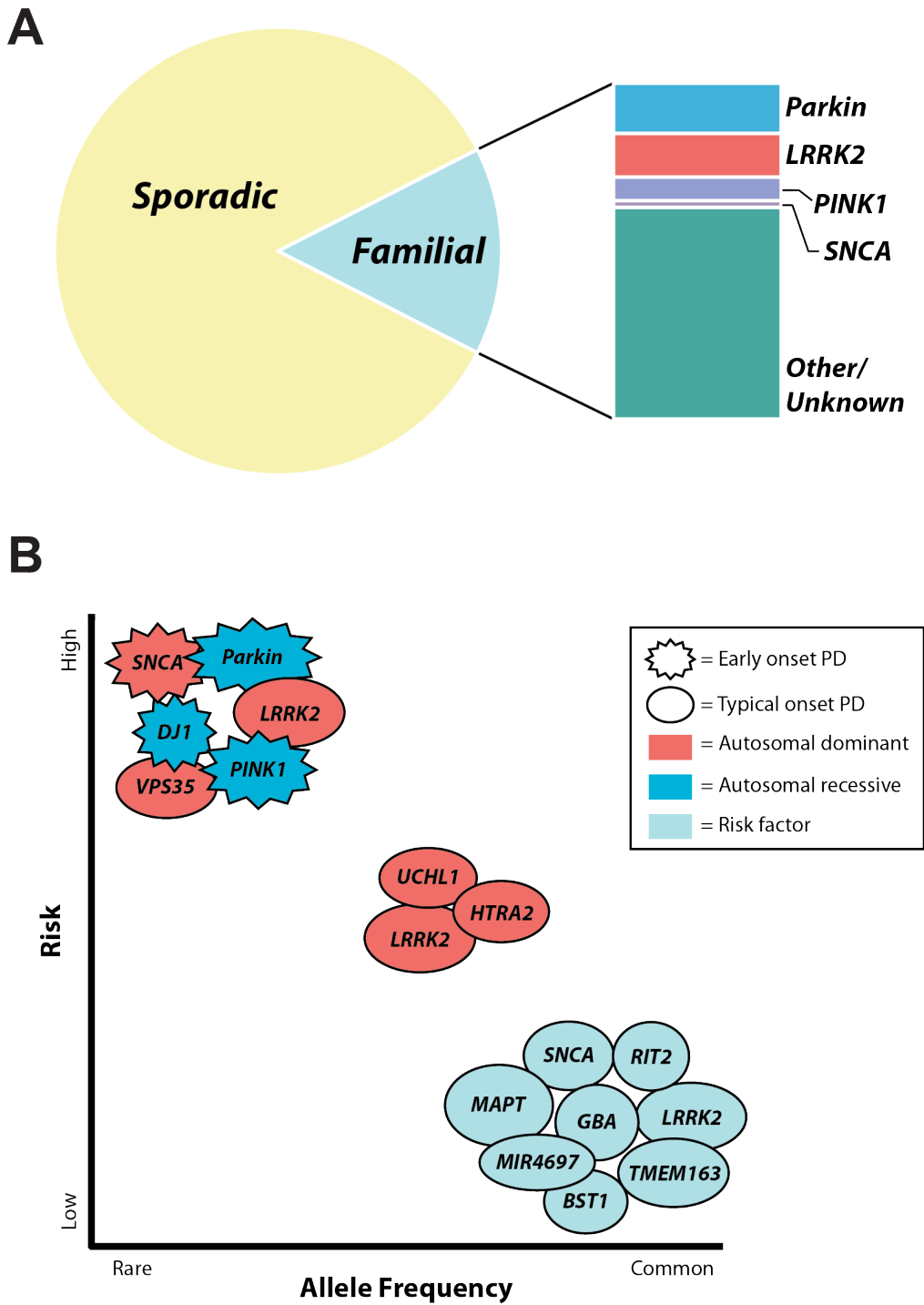
Figure 1.1. PD genetics. (A) Representation of PD causes. Approximately 90% of PD cases are sporadic. Parkin is the most common cause of familial PD, followed closely by LRRK2. (B) Genetic architecture of PD showing three classes of PD-related genes: Mendelian genes (rare alleles/high risk), moderate risk loci (medium frequency/medium risk), and low relative risk loci (common alleles/low risk; only a small fraction of genes are shown). Of the Mendelian genes, Parkin, PINK1, DJ1, and SNCA all cause early onset PD. VPS35, LRRK2, and SNCA are autosomal dominant. Adapted from [6, 21].

Table 1.1. PARK loci associated with familial PD[^]

PARK ID	Locus	Gene	Onset	Inheritance
PARK1/4	4q21-22	SNCA	Early	Autosomal Dominant
PARK2	6q25-27	PARKIN	Early	Autosomal Recessive
PARK3	2p13	Unknown	Typical	Autosomal Dominant
PARK5	4p13	UCHL1	Typical	Autosomal Dominant
PARK6	1p35-36	PINK1	Early	Autosomal Recessive
PARK7	1p36	DJ-1	Early	Autosomal Recessive
PARK8	12q12	LRRK2	Typical	Autosomal Dominant/Risk Factor
PARK9	1p36	ATP13A2	Early	Autosomal Recessive
PARK10	1p32	Unknown	Unknown	Risk Factor
PARK11	2q36-37	Unknown	Unknown	Risk Factor
PARK12	Xq21-25	Unknown	Unknown	Risk Factor
PARK13	2p12-13	HTRA2	Typical	Risk Factor
PARK14	22q13	PLA2G6	Early	Autosomal Recessive
PARK15	22q12-13	FBXO7	Early	Autosomal Recessive
PARK16	1q32	Unknown	Unknown	Risk Factor
PARK17	16q12	VPS35	Typical	Autosomal Dominant
PARK18	3q27	EF4G1	Typical	Autosomal Dominant
PARK19	1p21	DNAJC6	Early	Autosomal Recessive
PARK20	21q22	SYNJ1	Early	Autosomal Recessive
PARK21	3q22	DNAJC13	Typical	Autosomal Dominant
PARK22	7p11	CHCHD2	Unknown	Risk Factor
PARK23	15q22	VPS13C	Early	Autosomal Recessive

^ Adapted from [6, 10]

LRRK2

LRRK2 mutations are the most common known cause of PD, appearing in both familial and sporadic cases, and unlike most other Mendelian forms of the disease, LRRK2 patients present identically to those with idiopathic PD [22]. Together, these findings strongly suggest that understanding LRRK2 and LRRK2-derived PD may help with unraveling PD more broadly, including the vast majority of PD cases, which are not genetic. Thus, there has been a lot of active research on LRRK2 since its identification in 2004 [16, 17], and while some is known about the protein, there are also a lot of fundamental questions still to be answered.

Structure

LRRK2 is a 286 kDa polypeptide with multiple protein-protein interaction domains – including N-terminal armadillo, ankyrin, and LRR domains, and a C-terminal WD40 domain – that flank enzymatically active Roc (Ras of complex) GTPase, COR (C-terminal of Roc), and kinase domains (Figure 1.2) [23]. Mendelian PD-causing mutations in LRRK2 fall in the catalytic domains, including R1441C/G/H mutations in the Roc domain, Y1699C mutations in the COR domain, and G2019S and I2020T mutations in the kinase domain (Figure 2.1) [16]. The G2019S mutation, which falls in the kinase activation loop, is the most common LRRK2 PD mutation [2]. LRRK2 dimerizes through its GTPase domains, which is thought to regulate kinase activity, and R1441 mutations appear to fall in the hydrophobic dimer interface [24]. While most research interest has focused on the enzymatic domains and function of LRRK2, there are also reasons to be interested in understanding the N- and C-terminal parts of the protein. A mutation in the WD40 domain, G2385R, is known to be an intermediate risk factor for PD [25]. Interestingly, different mutations in LRRK2's WD40 domain lead to increased LRRK2 turnover and are linked to inflammatory diseases, including leprosy and Crohn's disease [26, 27]. The N-terminal protein-protein interacting domains are also of interest, as this region is divergent from the homolog LRRK1, which is not associated with disease risk [28].
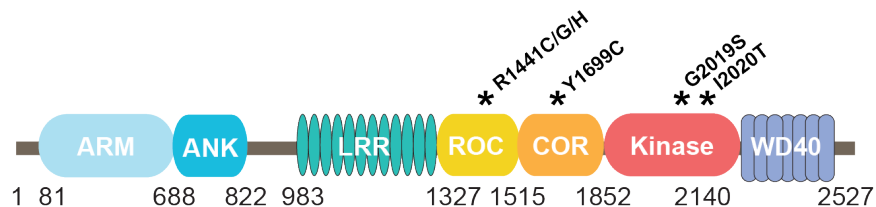
Figure 1.2. LRRK2 structure. Diagram of LRRK2 protein domains: Armadillo repeat (ARM) domain, Ankyrin repeat (ANK) domain, Leucine Rich Repeat (LRR) domain, Roc/COR GTPase domains, Kinase domain, and WD40 domain. Mendelian PD-associated point mutations are shown above the domains.

Wild type LRRK2 function

LRRK2 has been challenging to study, in part due to its size and complexity. It is difficult to isolate the functions of each part of the protein, and it has also been a technical hurdle to express and purify both *in vivo* and *in vitro* [22]. Furthermore, LRRK2 is lowly expressed across tissues and cell lines, making endogenous detection and characterization extremely difficult [1]. Interestingly, LRRK2 is expressed throughout the body, including the brain, but is not especially abundant in dopaminergic neurons [1]. Kidneys, lungs, and immune cells seems to express the greatest levels of LRRK2 [20]. Fitting with this observation, mice with LRRK2 knocked out appear to show no obvious brain phenotype, but do develop pathologies in their kidneys and lungs, which appear to be based on dysregulation of autophagy/lysosomal pathways [29, 30]. These findings suggest that wild type (WT) LRRK2 is essential, at least in some tissues, and may be an important regulator of autophagy, but they do not suggest an obvious role for LRRK2 in neurodegeneration. Adding to the difficulty in modeling LRRK2-driven PD, invertebrate model organisms like *C. elegans* and *Drosophila* only have a single LRRK homolog, and it is structurally more similar to human LRRK1 than LRRK2 [23].

Due to the difficulties of working with LRRK2, most studies aiming to understand LRRK2's localization, binding partners, turnover, and kinase activity have relied on over-expression [31]. However, while imperfect, over-expression data have led to a number of important discoveries on LRRK2 regulation and function. In terms of localization, over-expressed LRRK2 is generally seen as diffusely cytoplasmic, although with fractions of total LRRK2 found associated with microtubules, vesicles, mitochondria, and lysosomes [31, 32]. In the cytoplasm, LRRK2 is known to interact with 14-3-3 proteins [20, 33, 34]. LRRK2 has also been found to interact with microtubules, where it may regulate tubulin acetylation and/or

phosphorylate microtubule-associated protein Tau [35-37]. As described above, LRRK2 is thought to have functional relevance in autophagy, and is known to interact with autophagic receptor protein p62 [38]. LRRK2 has also been connected to mitophagy, in part through its roles in autophagy and microtubule-dependent transport [31]. Recently, a subset of Rab proteins were identified as LRRK2 substrates via phosphoproteomics, which has been a breakthrough in the field [39]. Rab GTPases play a central role in vesicular trafficking, and this interaction may account for LRRK2's known association with membrane-bound compartments [31, 40].

This finding has also helped resolve a longstanding search for bona fide LRRK2 substrates beyond LRRK2 auto-phosphorylation [41]. However, the regulation of LRRK2 kinase activity is still poorly understood. LRRK2 is basally phosphorylated at a number of N-terminal residues, and this phosphorylation is associated with LRRK2 activity (i.e. loss of phosphorylation on these residues is inhibitory) [42]. Rab29 has been identified as an upstream regulator of LRRK2 kinase activity, but the kinases and phosphatases responsible for maintaining the phosphorylation state of these regulatory residues have not been identified [43]. In general, regulators of LRRK2 activity and localization are not known, and signaling pathways downstream of LRRK2 are still in the early stages of characterization.

Mutant LRRK2 function

While the function of WT LRRK2 remains mostly a mystery, many groups have sought to determine what affect LRRK2 mutations have on the protein and the intracellular processes to which it is linked. As with investigations of WT LRRK2, animal models have been developed in hopes of finding mutant LRRK2 phenotypes relevant to PD. In general, transgenic animals do not display dopaminergic neuron loss [32]; however, there are some neuron-specific phenotypes

that have been observed. The most consistent phenotype is reduced neurite outgrowth observed in neurons expressing PD-mutant LRRK2 [44, 45]. However, this doesn't appear to necessarily be a mutation-dependent function, as neurite outgrowth defects have also been observed from WT LRRK2 over-expression [46]. Interestingly, LRRK2 models in *Drosophila* do exhibit age-dependent neuron loss, but this likewise occurs with both mutant and WT LRRK2, although the phenotypes are exacerbated by mutant forms of the protein [47, 48].

In vitro kinase assays have been used to show that LRRK2 PD mutations cause an increase in kinase activity [49]. With the discovery of LRRK2 substrates, this finding has been confirmed as LRRK2 mutations lead to both increased auto-phosphorylation and increased phosphorylation of Rab substrates [39, 41]. In theory, Rab hyper-phosphorylation could result in altered vesicular trafficking, potentially resulting in neuron death, although the pathways that would explain this form of toxicity are not yet established, and it is not immediately clear how this mechanism would take decades to manifest. As an alternative theory, there are published data that find that total LRRK2 protein levels, not kinase activity, account for neuronal cell death [50], and that LRRK2 mutants are degraded particularly poorly via autophagy [51], which could account for their toxicity. This theory fits with the knowledge that protein homeostasis (proteostasis) declines with aging, leading to an accumulation of excessive or damaged proteins in a number of diseases of aging [52]. A third theory is that LRRK2 mutants associate with different proteins, and these aberrant interactions lead to disease through dysregulation of LRRK2's kinase signaling or an altered role for LRRK2 as a scaffold. In support of this theory, LRRK2 mutations disrupt 14-3-3 binding [53, 54]. Some LRRK2 mutants also associate more strongly with microtubules [55], a phenomenon that could relate to dopaminergic susceptibility to LRRK2 mutations [56]. Ultimately, all of these theories may play some role in LRRK2-

driven PD, but we do not currently know enough about WT LRRK2 function or the affects of LRRK2 mutations to deeply understand disease etiology.

CHAPTER II: TRIM1 BINDS LRRK2 AND REGULATES ITS MICROTUBULE LOCALIZATION

Introduction

LRRK2 is a large and complex protein with numerous protein-protein interaction domains flanking a central catalytic core [57, 58]. While its expression appears to be essential for many cells [30, 59], LRRK2's primary roles have largely remained a mystery since LRRK2 was identified. In order to gain insight into pathways LRRK2 may be involved in, several groups have performed various screens to identify interacting proteins [60-62]. While these screens have successfully identified some LRRK2 interactors, they have potentially missed important interactors because they didn't use full length LRRK2 or relied on yeast two-hybrid systems instead of *in vivo* interactions identified from human cells. Here, we use mass spectrometry with full-length LRRK2 in human HEK-293T cells to identify new interacting proteins.

In addition to identifying signaling pathways and cellular processes in which LRRK2 is involved, identifying interactors can also give information on LRRK2 localization. There is at least some data showing LRRK2 localization at just about every cellular compartment, but the strongest evidence supports LRRK2's diffuse localization in the cytoplasm, association with membrane-bound structures, and co-localization with microtubules. In some cases, LRRK2 interactors in a particular cellular compartment are known, such as 14-3-3 proteins in the cytoplasm [63], or some members of the Rab family at membranes. However, upstream signals

or binding partners responsible for LRRK2 localization to microtubules have not yet been identified. Notably, many pathological effects of LRRK2 mutants appear to be directly related to cytoskeletal dysfunction. For example, the best-characterized phenotype in models of LRRK2 PD is neurite outgrowth defects. Developing neurons overexpressing G2019S mutant LRRK2 grow short, poorly branched neurites [45, 64]. Inversely, LRRK2-deficient neurons grow longer processes than normal neurons [44], suggesting that WT LRRK2 plays a critical role in regulating neurite outgrowth, a microtubule-dependent process. Moreover, the pathogenic R1441C LRRK2 mutant impairs axonal transport in *Drosophila* by associating with deacetylated microtubules in neurons [65]. Finally, with broad implications for neurodegeneration in general, cells expressing mutant LRRK2 have increased levels of phosphorylated microtubule-associated protein Tau, a key component of neurofibrillary tangles in numerous neurodegenerative diseases [66-68]. Together these findings suggest that LRRK2 activity plays an important role at microtubules in neurons, but technical limitations in the field have prevented a thorough investigation of this hypothesis.

We identified Tripartite Motif-Containing Protein 1 (TRIM1) as a novel LRRK2 interacting protein. TRIM1 is a virtually unstudied member of the large TRIM family. Like all TRIMs, TRIM1 contains an N-terminal RING domain, B-Box domains, and a Coiled-Coil domain (Figure 2.1). Additionally, TRIM1 contains a COS box in its C-terminus, which facilitates TRIM1 binding to microtubules [69]. TRIM1 is expressed most highly in brain, kidney, and heart tissues [70]. Point mutations in TRIM1 that abolish its microtubule localization cause a rare form of X-linked mental retardation in humans, suggesting that TRIM1 is functionally important in the brain [71]. TRIM1 is a putative E3 ubiquitin ligase that has not previously been linked to LRRK2 biology.
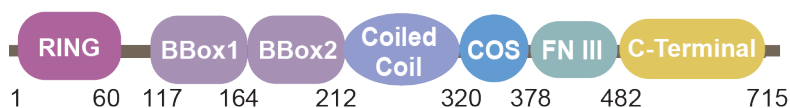
Figure 2.1. TRIM1 structure. Diagram of TRIM1 protein domains: a RING domain, two B-Box domains, a Coiled-Coil domain, a microtubule-binding COS box, a Fibronectin III domain, and the far C-terminus of the protein.

Results

TRIM1 is a novel LRRK2 interacting partner

To identify LRRK2-interacting protein, we collaborated with Nevan Krogan's lab at UCSF to perform affinity purification-mass spectrometry (AP-MS) on full-length FLAG-tagged LRRK2 exogenously expressed in HEK-293T cells. FLAG-LRRK2 or a FLAG control vector was transiently transfected into HEK-293T cells, and then affinity purified with an anti-FLAG antibody from lysates and subjected to mass spectrometry in the Krogan lab as previously described [72-75]. LRRK2 interactors were defined as proteins with at least three-fold increased abundance in FLAG-LRRK2 eluates versus FLAG-controls samples. This screen identified 25 previously published interacting proteins, as well as 48 novel interactors (Figure 2.2A, Table 2.1). The top hit is Tripartite Motif-Containing Protein 1 (TRIM1, also called MID2).

To verify that TRIM1 and LRRK2 interact, we exogenously expressed Myc-TRIM1 and FLAG-LRRK2 in HEK-293T cells. When LRRK2 was pulled down from these lysates, TRIM1 readily co-immunoprecipitated (Figure 2.2B). TRIM1 and LRRK2 are both expressed at low levels endogenously in most cell lines and tissue types, and neither is easily detectable in lysates from most common cell lines. However, when endogenous TRIM1 was immunoprecipitated

from HEK-293T lysates, endogenous LRRK2 is detectable in the eluate (Figure 2.2C). Thus, we

confirmed that endogenous TRIM1 and LRRK2 interact under physiological conditions, as well.
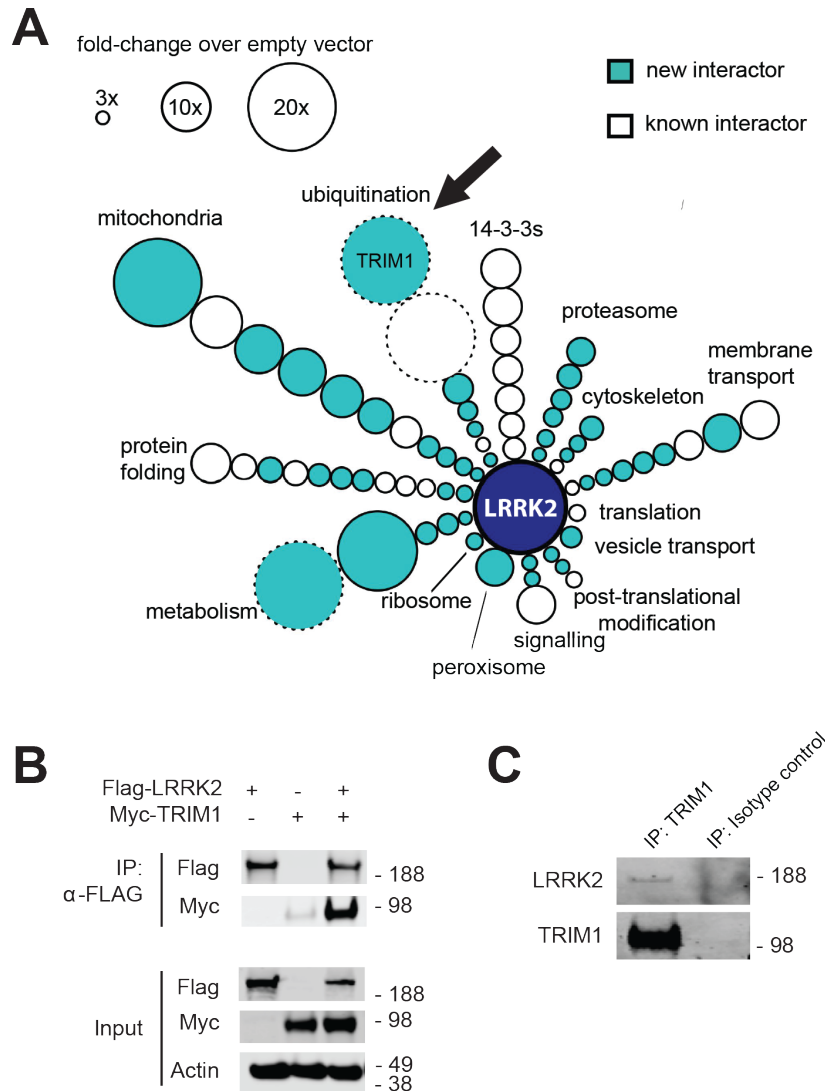
Figure 2.2. TRIM1 is a newly identified LRRK2 interacting protein. (A) LRRK2 interactome found by AP-MS in HEK-293T cells. LRRK2 interacting partners are classified radially by function. The size of the circle represents the fold-change of LRRK2-associated peptide abundance over empty FLAG-vector. Dashed black outlines indicate that no peptides were found in empty vector control samples.   Teal indicates novel interactors and white is previously identified interactors. The arrow marks TRIM1, the highest confidence hit. (B) Co-immunoprecipitation of Myc-TRIM1 with FLAG-LRRK2 from HEK-293T cells.   (C) Co-immunoprecipitation of endogenous LRRK2 with endogenous TRIM1 from HEK-293T cells.

Table 2.1. LRRK2 interacting partners

Uniprot ID	Gene Name	Fold Change	Functional Group	Previously Reported?
Q5S007	LRRK2	76.586	BAIT	Y
Q9UJV3	MID2	***	Ubiquitination	N
O95714	HERC2	***	Ubiquitination	Y
A1L0T0	ILVBL	***	Metabolism	N
Q9Y241	HIGD1A	20.734	Mitochondria	N
Q15366	PCBP2	20.700	Ubiquitination	N
P51648	ALDH3A2	18.744	Metabolism	N
Q96TA2	YME1L1	12.143	Mitochondria	Y
O43819	SCO2	11.352	Mitochondria	N
P07919	UQCRH	11.079	Mitochondria	N
P08574	CYC1	9.871	Mitochondria	N
P31947	SFN, YWHAS	9.241	14-3-3	Y
Q9UL15	BAG5	9.239	Protein folding	Y
P61981	YWHAG	9.062	14-3-3	Y
Q9H936	SLC25A22	8.935	Membrane transport	Y
P06493	CDC42	8.927	Signaling	Y
Q6P1M0	SLC27A4	8.804	Membrane transport	N
P28288	ABCD3	8.727	Peroxisome	N
O75880	SCO1	8.215	Mitochondria	N
Q9Y4W6	AFG3L2	7.251	Mitochondria	Y
Q7Z6Z7	HUWE1	6.998	Ubiquitination	N
P31946	YWHAB	6.860	14-3-3	Y
P62258	HEL2,YWHAE	6.811	14-3-3	Y
P05141	SLC25A5	6.730	Membrane transport	Y
P63104	YWHAZ	6.642	14-3-3	Y
P28074	PSMB5	6.548	Proteasome	N
Q13501	SQSTM1	5.870	Protein folding	Y
Q13451	FKBP5	5.867	Protein folding	N
Q04917	YWHAH	5.738	14-3-3	Y
O95816	BAG2	5.711	Protein folding	Y
P51665	PSMB4	5.600	Proteasome	N
Q07065	CKAP4	5.469	Cytoskeleton	N
Q14318	FKBP8	5.170	Protein folding	N
P27348	YWHAQ	5.091	14-3-3	Y
Q8WVX9	FAR1	5.045	Metabolism	N
P07900	HSP90AA1,EL52	5.034	Protein folding	Y
Q00325	SLC25A3	5.019	Membrane transport	N
P51970	NDUFA8	4.997	Mitochondria	N
Q58FF8	HSP90AB2P	4.984	Protein folding	N

Uniprot ID	Gene Name	Fold Change	Functional Group	Previously Reported?
P49755	TMED10	4.903	Vesicle transport	N
Q9NZ01	TECR	4.876	Metabolism	N
Q02978	SLC25A11	4.874	Membrane transport	N
P53985	SLC16A1	4.734	Membrane transport	N
P20618	PSMB1	4.677	Proteasome	N
P08238	HSP90AB1	4.673	Protein folding	Y
Q16543	CDC37	4.511	Protein folding	Y
O00483	NDUFA4	4.510	Mitochondria	N
Q9Y2Z0	SUGT1	4.505	Ubiquitination	N
P60900	PSMA6	4.400	Proteasome	N
O00217	NDUFS8	4.082	Mitochondria	N
P31689	DNAJA1	4.015	Protein folding	Y
P28072	PSMB6	3.939	Proteasome	N
Q9UKD2	MRTO4	3.822	Ribosome	N
Q3ZCQ8	TIMM50	3.821	Membrane transport	N
Q69YQ0	SPECC1L	3.797	Cytoskeleton	N
Q99615	DNAJC7	3.785	Protein folding	N
O60884	DNAJA2	3.759	Protein folding	N
Q9Y285	FARSLA,FARSA	3.738	Translation	Y
P51571	SSR4	3.663	Post-translation modification	Y
Q9Y5V3	MAGED1	3.560	Ubiquitination	N
P53041	PPP5C	3.545	Signaling	N
P62873	GNB1	3.479	Signaling	N
O60762	DPM1	3.479	Post-translation modification	N
Q9UBX3	SLC25A10	3.243	Membrane transport	N
P35613	BSG,HEMMPRIN	3.237	Post-translation modification	N
Q9UNE7	STUB1	3.184	Ubiquitination	Y
P12236	SLC25A6	3.145	Membrane transport	Y
P49721	PSMB2	3.123	Proteasome	N
Q3ZCM7	TUBB8	3.110	Cytoskeleton	N
P50402	EMD	3.047	Cytoskeleton	Y
O43164	PJA2	3.035	Ubiquitination	N
Q9NVI7	ATAD3A	3.020	Mitochondria	N
Q15181	PPA1	3.018	Metabolism	N
P19474	TRIM21	3.000	Ubiquitination	N

*** = Proteins had no peptides in empty vector control sample

TRIM1 co-localizes with LRRK2 at microtubules

While not much is known about TRIM1, it has been previously published that the protein localizes to microtubules [76]. Multiple groups have found that LRRK2, at least in part, associates with microtubules [35, 36], and that some LRRK2 PD mutations or kinase inhibition can increase the fraction of LRRK2 found at microtubules [55, 65]. However, the molecular mechanism for regulating LRRK2 localization is not well understood. To determine if LRRK2 co-localizes with TRIM1 at microtubules, we used live cell confocal microscopy to examine the subcellular distribution of LRRK2 in human lung H1299 cells. We expressed GFP-LRRK2 with either mCherry-Tubulin or mCherry-TRIM1. We verified previous findings that over-expressed LRRK2 is generally diffusely cytoplasmic, with only a small fraction localizing to microtubules when co-expressed with mCherry-Tubulin (Figure 2.3A). Remarkably, however, we found that co-expression of TRIM1 led the vast majority of LRRK2 to localize to microtubules (Figure 2.3B). Interestingly, while mCherry-TRIM1 coated microtubules smoothly (Figure 2.3B, left panel, inset), GFP-LRRK2 appeared more punctate and discontinuous (Figure 2.3B, middle panel, inset), suggesting that LRRK2 may form multi-protein complexes at the microtubule with additional binding partners beyond TRIM1. These observations held true across all cell lines examined (Figure 2.4).

Repeated attempts to visualize the subcellular localization of endogenous LRRK2 using live cell confocal microscopy or immunofluorescence did not yield a LRRK2-specific signal. Live cell imaging was performed using CRISPR GFP-tagged LRRK2 in A549 cells (gift of Dario Alessi) and CRISPR GFP-tagged LRRK2 in HEK-293T cells (created in our lab). Immunofluorescence was performed on the preceding CRISPR GFP-LRRK2 lines as well as A549 LRRK2 WT compared to CRISPR knockout (gift of Dario Alessi), murine RAW 264.7

macrophages wild type versus TALEN knockout (MJFF), and human melanoma Malme-3M wild type compared to siRNA knockdown using a variety of LRRK2 antibodies (MJFF C41-2, UDD3, N231). The inability to reproducibly visualize endogenous LRRK2 using these methods is in keeping with previous reports and highlights an important limitation in the field.
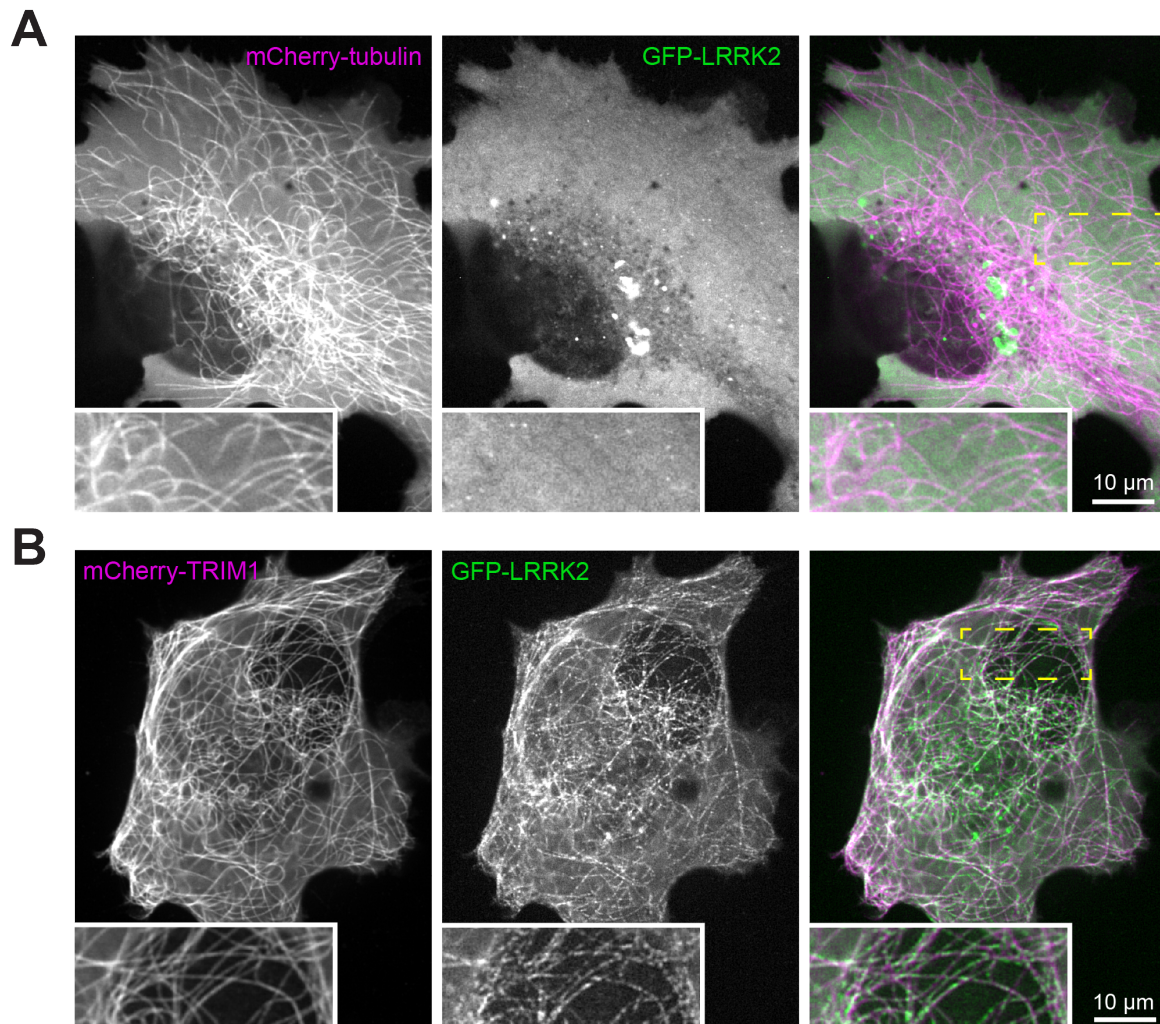
Figure 2.3. TRIM1 co-expression recruits LRRK2 to the microtubule. (A) Live-cell confocal microscopy of GFP-LRRK2 and mCherry-Tubulin transiently transfected into H1299 cells. In the presence of mCherry-Tubulin, GFP-LRRK2 is diffusely cytoplasmic. From left to right: mCherry-Tubulin, GFP-LRRK2, merged image. Inset shows higher magnification of region identified by box in merged image. (B) In the presence of mCherry-TRIM1, GFP-LRRK2 localizes to the microtubule. From left to right: mCherry-TRIM1, GFP-LRRK2, merged image. Inset shows higher magnification of region identified by box in merged image.
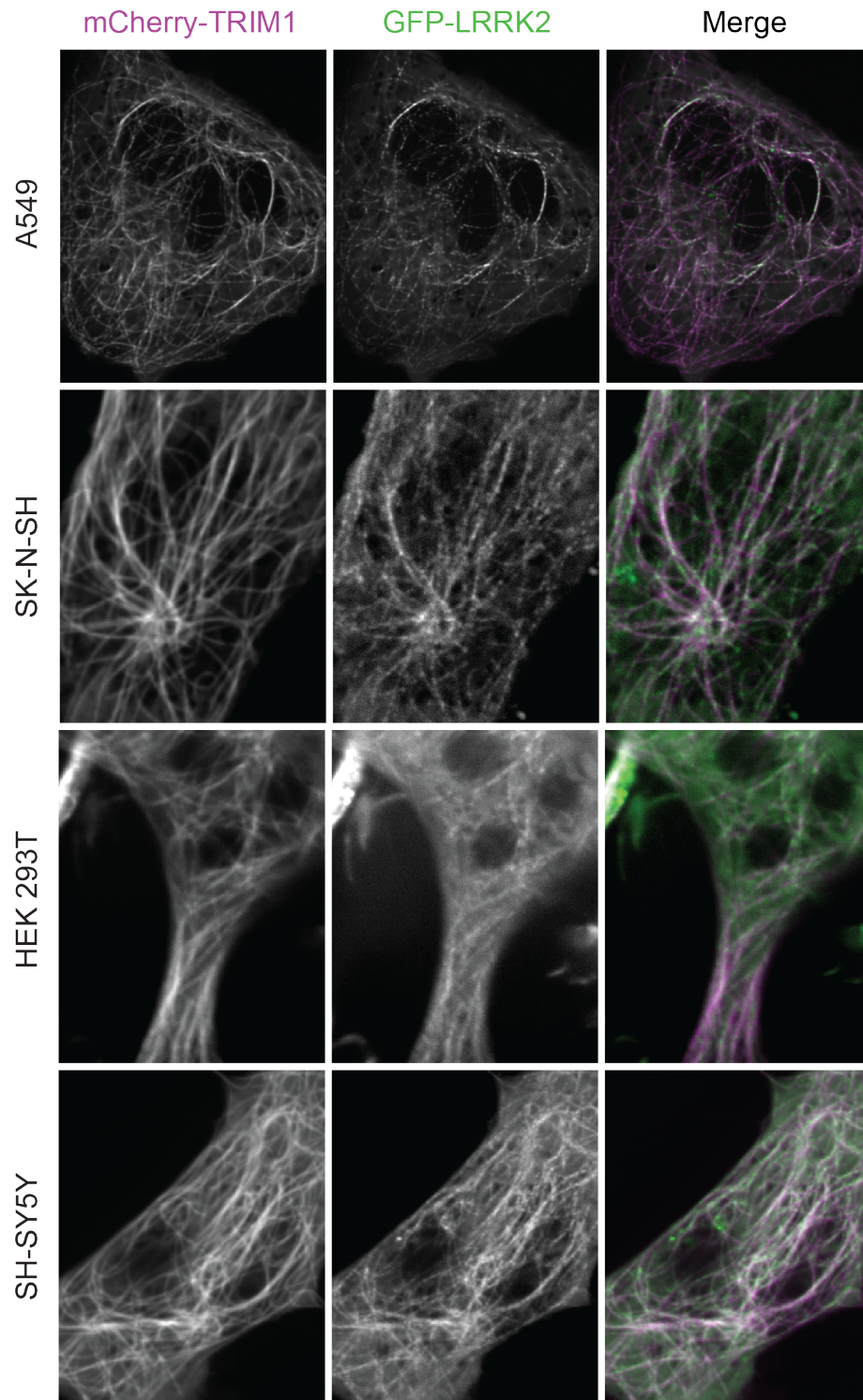
Figure 2.4. LRRK2 co-localizes with TRIM1 at microtubules across cell lines.
Live-cell confocal microscopy of GFP-LRRK2 and mCherry-TRIM1 transiently transfected into various cell lines. From top to bottom: A549 cells (human lung carcinoma), SK-N-SH cells (human neuroblastoma), HEK-293T cells (human embryonic kidney), and SY-SY5Y cells (human neuroblastoma). Each row, from left to right: mCherry-TRIM1, GFP-LRRK2, merged image.

TRIM18 (also called MID1) is highly homologous to TRIM1 (Figure 2.5A). Like TRIM1, TRIM18 is known to associate with microtubules [69]. However, we found that Myc-TRIM18 did not robustly co-immunoprecipitate with LRRK2 (Figure 2.5B). Furthermore, LRRK2 did not co-localize with TRIM18 at microtubules as it does with TRIM1 (Figure 2.5C). Thus, it appears the LRRK2-TRIM1 interaction is highly specific.

TRIM1 competes with 14-3-3 proteins to bind a regulatory loop on LRRK2

To better characterize the LRRK2-TRIM1 interaction, we performed a series of co-immunoprecipitation experiments with various truncated forms of both LRRK2 and TRIM1. By immunoprecipitating truncated variants of TRIM1 and immunoblotting for LRRK2 association, we found that the B-Box domain of TRIM1 is required for LRRK2 binding (Figure 2.6A). As shown in Figure 2.5, this domain contains a region that is substantially divergent from TRIM18, which likely accounts for the difference in ability to bind LRRK2 between the two homologous TRIM proteins.

Conversely, by immunoprecipitating LRRK2 truncated constructs, we identified the region between the Ankyrin and LRR domains (amino acids 822-982) as essential for TRIM1 binding (Figure 2.6B). Furthermore, this region is necessary and sufficient for TRIM1-mediated LRRK2 localization to microtubules (Figure 2.6C). This region is predicted to be highly unstructured and solvent-exposed based on *in silico* modeling. Notably, this region is known to contain a number of serine residues that are phosphorylated by upstream kinases, causing LRRK2 kinase activation [42]. These data suggest that this region may be a critical site of LRRK2 regulation by external factors, potentially including TRIM1. Thus, we term $LRRK2_{822-982}$ the LRRK2 Regulatory Loop (RL) (Figure 2.6D).

A

Ring Finger

```
TRIM18    1  METLESELTCPICLELFEDPLLLPCAHSLCFNCAHRILVSHCATNESVESITAFQCPTCR
TRIM1     1  METLESELTCPICLELFEDPLLLPCAHSLCFSCAHRILVSSCSSGESIEPITAFQCPTCR
```

linker and B-box1

```
TRIM18   61  HVIILSQRGLDGLKRNVTLQNIIDRFQKASVSGPNSPSETRRERAEDANTMTSAEKVLCQ
TRIM1    61  YVISLNHRGLDGLKRNVTLQNIIDRFQKASVSGPNSPSESRRERTYRPTTAMSSERIACQ
```

B-box2

```
TRIM18  121  FCDQDPAQDAVKTCVTCEVSYCDECLKATHPNKKPFTGHRLIEPIPDSHIRGLMCLEHED
TRIM1   121  FCEQDPPRDAVKTCITCEVSYCDRCLRATHPNKKPFTSHRLVEPVPDTHLRGITCLDHEN
```

Coiled coil

```
TRIM18  181  EKVNMYCVTDDQLICALCKLVGRHRDHQVAALSERYDKLKQNLESNLTNLIKRNIELETL
TRIM1   181  EKVNMYCVSDDQLICALCKLVGRHRDHQVASLNDRFEKLKQTLEMNLTNLVKRNSELENQ
```

Coiled coil

```
TRIM18  241  LAKLIQTCQHVEVNASRQEAKITEECDLLIEIIQQRRQIIGTKIKEGKVMRLRKLAQQIA
TRIM1   241  MAKLIQICQQVEVNTAMHEAKLMEECDELVEIIQQRKQMIAVKIKETKVMKLRKLAQQVA
```

Coiled coil

```
TRIM18  301  NCKQCIERSASLISQAEHSLKENDHARFLQTAKNITERVSMATASSQVLIPEINLNDTFT
TRIM1   301  NCRQCLERSTVLINQAEHILKENDQARFLQSAKNIAERVAMATASSQVLIPDINFNDAFE
```

Fibronectin III

```
TRIM18  361  TFALDFSREKKLLEGLDYLTAPNPPIIREELCTASYDTITVHWTSDDEFSVVSYELQYTI
TRIM1   361  NFALDFSREKKLLEGLDYLTAPNPPSIREELCTASHDTITVHWTSDDEFSISSYELQYTI
```

Fibronectin III

```
TRIM18  421  FTGQANVVSLCNSADSWMIVPNIKQNHYTVHGLQSGTKYIFMVKAINQAGSRSSEFGRLK
TRIM1   421  FTGQANFISLYNSVDSWMIVPNIKQNHYTVHGLQSGTRYIFIVKAINQAGSRNSEPTRLK
```

C-terminal domain (SPRY)

```
TRIM18  481  TNSQPFKLDPKSAHRKLKVSHDNLTVERDESSSKKSHTPERFTSQGSYGVAGNIFIDSGR
TRIM1   481  TNSQPFKLDPKMTHKKLKISNDGLQMEKDESSLKKSHTPERFSGTGCYGAAGNIFIDSGC
```

C-terminal domain (SPRY)

```
TRIM18  541  HYWEVVISGSTWYAIGLAYKSAPKHEWIGKNSASWALGRCNNNWVVRHNSKEIPIEPAPH
TRIM1   541  HYWEVVMGSSTWYAIGIAYKSAPKNEWIGKNASSWVFSRCNSNFVVRHNNKEMLVLVPPH
```

C-terminal domain (SPRY)

```
TRIM18  601  LRRVGILLDYDNGSIAFYDALNSIHLYTFDVAFAQPVCPTFTVWNKCLTIITGLPIPDHL
TRIM1   601  LKRLGVLLDYDNNMLSFYDPANSLHLHTFDVTFILPVCPTFTIWNKSLMILSGLPAPDFI
```

```
TRIM18  661  DCTEQLP------------------
TRIM1   661  DYPERQECNCRPQESPYVSGMKTCH
```

B

FLAG-LRRK2	+	+
Myc-TRIM18	−	+
Myc-TRIM1	+	−

IP: α-FLAG — FLAG - 188; Myc - 98

Input — FLAG - 188; Myc - 98; Actin - 38

C

mCherry-TRIM18   GFP-LRRK2

10 µm
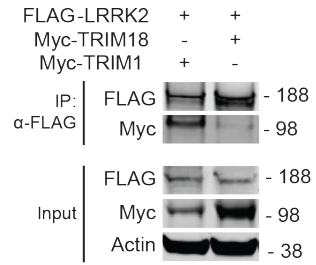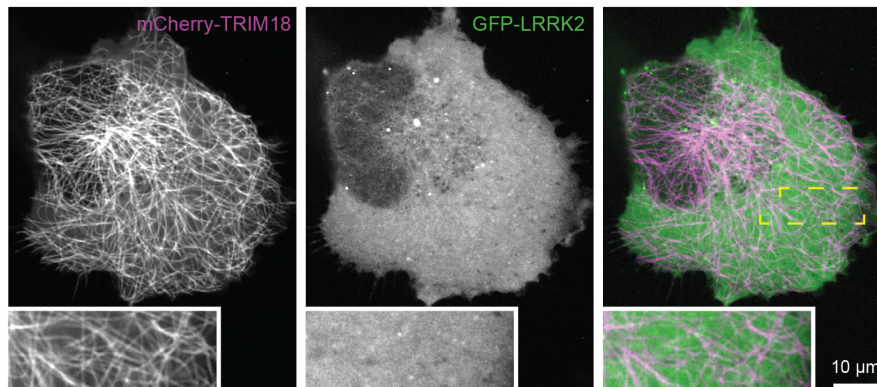
Figure 2.5. The LRRK2-TRIM1 interaction is highly specific. (A) Alignment of TRIM18 with TRIM1. Domains are labeled above alignment. Red line designates region required for TRIM1 interaction with LRRK2. Double red line designates region of least homology in the B-box domain. (B) Immunoprecipitation of GFP-LRRK2 with either Myc-TRIM1 or Myc-TRIM-18. (C) Live-cell confocal microscopy of GFP-LRRK2 and mCherry-TRIM18 transiently transfected into H1299 cells. From left to right: mCherry-TRIM18, GFP-LRRK2, merged image. Inset shows higher magnification of region identified by box in merged image.

21
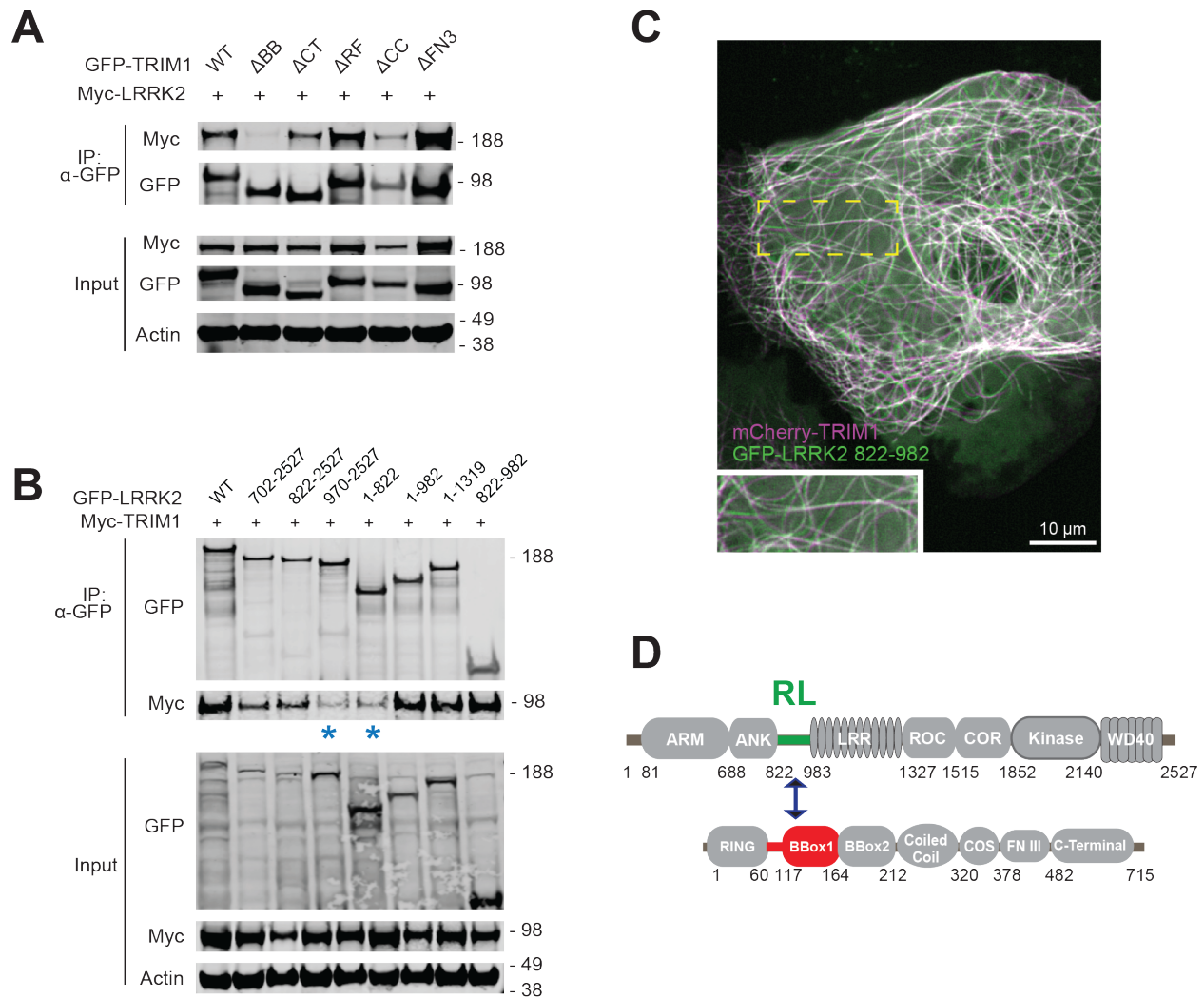
Figure 2.6. TRIM1 binds a LRRK2 regulatory loop region via its B-box domain. (A) Co-immunoprecipitation of full-length myc-LRRK2 with GFP-TRIM1 domain constructs in HEK-293T cells (ΔBB: TRIM1 construct lacking both B-box domains; ΔCT: TRIM1 lacking C-terminal domain, ΔRF: TRIM1 lacking ring-finger domain; ΔCC: TRIM1 lacking coiled coil domain; ΔFN3: TRIM1 lacking fibronectin III domain; details of constructs in [69]). (B) Co-immunoprecipitation of full-length myc-TRIM1 with GFP-LRRK2 domain constructs in HEK-293T cells. LRRK2$_{822-892}$ is necessary and sufficient for interaction with TRIM1. (C) Live-cell confocal microscopy of GFP-LRRK2$_{822-982}$ and mCherry-TRIM1 transiently transfected into H1299 cells. (D) Schematic of LRRK2-TRIM1 interaction mediated by the LRRK2 Regulatory Loop (LRRK2$_{822-982}$ (green)), labeled "RL" and TRIM1$_{BBox1}$ (red).

The RL is already known to be a binding region for cytoplasmic 14-3-3 proteins, one of the best-characterized classes of LRRK2 interactors [33]. Because 14-3-3 binding has been shown to regulate LRRK2 cytoplasmic localization [63], we postulated that TRIM1 and 14-3-3

might compete for LRRK2 RL binding and correspondingly regulate LRRK2 localization. To test this, we co-expressed mCherry-TRIM1, GFP-LRRK2, and EBFP-14-3-3 theta in H1299 cells. We found that GFP-LRRK2 co-localized with mCherry-TRIM1 along microtubules, while EBFP-14-3-3 remained diffusely cytoplasmic (Figure 2.7A).

We further examined the ability of LRRK2 to co-immunoprecipitate with 14-3-3 in the presence and absence of TRIM1. GFP-LRRK2 co-immunoprecipitated V5-14-3-3 theta in the absence of Myc-TRIM1, as previously reported [63]; however, when Myc-TRIM1 was co-expressed, only 19% as much 14-3-3 was pulled down with LRRK2 (Figure 2.7B, quantified in Figure 2.7C). Additionally, because previous work has shown that LRRK2-14-3-3 binding requires several serine residues in the RL to be phosphorylated, including Ser910 and Ser935 [34, 54], we tested co-immunoprecipitation with a non-phosphorylatable LRRK2 S910A/S935A double mutant (LRRK2-SA). As expected, GFP-LRRK2-SA did not co-immunoprecipitate with 14-3-3, but still readily associated with TRIM1 (Figure 2.7B). This suggests that TRIM1 binding does not require phosphorylation of the LRRK2 RL, in contrast with 14-3-3.

We wanted to further assess the importance of LRRK2 phosphorylation in 14-3-3 versus TRIM1 binding. To do this, we pulled down LRRK2 bound to either 14-3-3 or TRIM1 by immunoprecipitating V5-14-3-3 or Myc-TRIM from HEK-293T cells. We then immunoblotted for total LRRK2, as well as phosphorylated species pS910 and pS935 (Figure 2.7D). LRRK2 Ser910 phosphorylation was 3.0-fold lower in the TRIM1-bound LRRK2 fraction, compared to 14-3-3 bound LRRK2, and Ser935 phosphorylation was similarly 4.4-fold lower with TRIM1 (Figure 2.7E). Thus, it appears that the phosphorylation status of the LRRK2 RL can determine LRRK's affinity for 14-3-3 or TRIM1 binding, and consequently, LRRK2 localization.
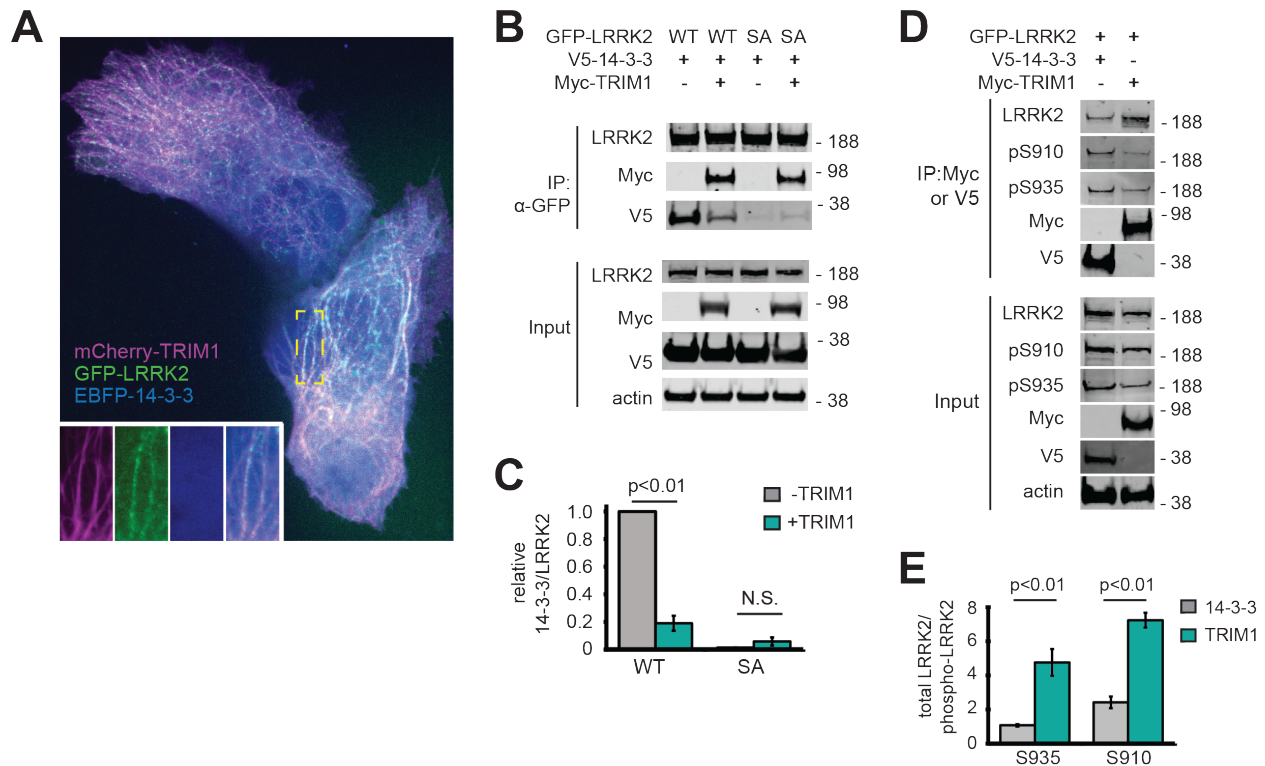
Figure 2.7. TRIM1 competes with 14-3-3 to bind the LRRK2 RL. (A) Live-cell confocal microscopy of GFP-LRRK2, mCherry-TRIM1, and EBFP-14-3-3 theta in H1299 cells. Inset shows higher magnification of region identified by box. From left to right: mCherry-TRIM1, GFP-LRRK2, EBFP-14-3-3, merged image. (B) Co-immunoprecipitation of GFP-LRRK2 wild type (WT) and Ser910Ala Ser935Ala (SA) with V5-14-3-3 theta in the presence and absence of myc-TRIM1 in HEK-293T cells. (C) Quantification of (B) showing the mean value from three experiments. (D) Co-immunoprecipitation of GFP-LRRK2 with either V5-14-3-3 theta or myc-TRIM in HEK-293T cells. Blot shows total LRRK2, phospho-Ser910 LRRK2, and phospho-Ser935 LRRK2. (E) Quantification of (D) showing the mean value from three experiments.

Discussion

We performed a global AP-MS proteomic screen in HEK-293T cells to identify LRRK2 interactors. This robust screen identified numerous previously reported interactors, while also finding 48 novel interactors, including TRIM1, a barely-studied putative E3 ligase that associates with microtubules. Intriguingly, while TRIM1 has never been directly linked to LRRK2 or

Parkinson's biology before, the TRIM1 gene does fall in the PARK12 genomic locus on the X-chromosome [77]. This large locus contains at least 200 genes recognized by UniProt, and no single one has yet been definitively linked to Parkinson's, but our findings indicate that TRIM1 could be a relevant candidate.

We identified the region of LRRK2 where TRIM1 binds: a small, flexible region between the Ankyrin and LRR domains we have termed the LRRK2 Regulatory Loop (RL). This is notable because previous interactome studies have used truncated LRRK2 lacking the N-terminal portion of the protein because it is easier to work with [60, 61]. This could explain why previous work has missed TRIM1 as a strong interactor, along with potentially a number of other novel interactors identified by our screen using full-length LRRK2. Also of note, LRRK1, LRRK2's closest homolog, lacks a homologous RL region in its N-terminus [78]. Despite having highly similar catalytic domains, LRRK1 has no known PD-causing mutations. It is likely that LRRK2 and LRRK1 associate with different binding partners, such as TRIM1, and/or different cellular compartments, leading to their distinct roles in disease.

We found that TRIM1 expression leads to a remarkable change in LRRK2 localization, causing nearly all LRRK2 protein to co-localize with TRIM1 along microtubules. While LRRK2 has long been known to occasionally associate with microtubules [35], no interacting proteins have been seen to have the profound effect on LRRK2 localization that TRIM1 has. LRRK2 PD mutants and LRRK2 treated with kinases inhibitors have been found to associate more with microtubules than WT LRRK2 [55, 79]. This raises the possibility that TRIM1-mediated LRRK2 localization may be especially important in cases of PD mutants or small molecule-based inhibition, and TRIM1 itself could even be a therapeutic target in PD.

We also found that TRIM1 and 14-3-3 compete to bind the LRRK2 RL. Because TRIM1 is so lowly expressed in cell lines and tissues, we postulate that LRRK2 has generally been observed to be diffusely cytoplasmic because, without TRIM1 over-expression, there is simply not enough TRIM1 present in cells to bind and localize a sizeable fraction of exogenous LRRK2 to microtubules. However, our data suggest that when both 14-3-3 and TRIM1 are over-expressed with LRRK2, LRRK2 preferentially binds and localizes with TRIM1, and that this is at least partially dependent on the phosphorylation status of two serines within the RL (Ser910 and Ser935). 14-3-3 and TRIM1 competition *in vivo* may define two functionally distinct pools of LRRK2. Phosphorylation or dephosphorylation of these serines may act as a molecular switch regulating LRRK2's binding partners and localization, as well as associated downstream effects. This is, again, especially notable in the cases of LRRK2 PD mutants that associate more strongly with microtubules than WT, or in the case of kinase inhibition, where LRRK2 is observed to bind microtubules as well as undergo ubiquitination and subsequent degradation via a currently unknown E3 ubiquitin ligase.

To follow up on this work, there are a number of logical experiments to perform. For one, the microtubule-localized LRRK2 images (e.g. Figures 2.3 and 2.4) show LRRK2 coating microtubules in a punctate, discontinuous manner, suggesting that there may be proteins beyond TRIM1 present in a complex. Using a similar AP-MS approach, we could identify additional complex members that may give more insight into the functional significance of the LRRK2/TRIM1 interaction. Furthermore, even without performing more mass spectrometry, there are dozens more novel hits found in our initial screen to investigate. Those hits related to ubiquitination, the cytoskeleton, or the proteasome may be particularly worth pursuing. Finally, it would be interesting to quantitatively compare interactomes of WT LRRK2 to LRRK2 PD

mutants as a way of finding LRRK2-associated pathways that are altered in diseased states, as well as examining LRRK2 interactomes from different cell types and tissues.

CHAPTER III: TRIM1 REGULATES LRRK2 TURNOVER AND RESCUES PARKINSON'S DISEASE-RELATED PHENOTYPES

Introduction

Proteostasis is essential for maintaining functional and healthy cells, especially neurons, due to their long lifespans and inability to dilute aggregated proteins via cell division [80]. In fact, a hallmark of many neurodegenerative diseases is an accumulation of protein aggregates. In PD, α-synuclein is the classic protein found in Lewy body aggregates, often co-occurring with ubiquitin [81], a sign that protein degradation pathways have broken down during the course of disease. LRRK2 is also sometimes found in Lewy body aggregates in postmortem brains from PD patients [82]. Groups have observed that LRRK2 G2019S has a longer half-life in cells, further linking LRRK2 and PD to potentially abnormal proteostasis [51]. In fact, some have argued that increased LRRK2 protein levels in cells, not simply increased kinase activity, is essential for neurodegeneration [50]. Finally, adding an extra layer of interest to LRRK2 turnover specifically by the ubiquitin-proteasome system, LRRK2 kinase inhibitors cause LRRK2 to be ubiquitinated and degraded via the proteasome [42, 83].

Until our work, only three E3 ubiquitin ligases have been associated with LRRK2: (1) WSB1, which ubiquitinates LRRK2 via atypical K27 and K29 linkages and causes LRRK2 aggregation but does not appear to promote proteasomal degradation [61]; (2) HERC2, which appears to bind but not ubiquitinate LRRK2 [48]; and (3) CHIP, an HSP70 co-chaperone that interacts with many partially folded proteins and causes LRRK2 degradation via the proteasome [62, 84]. In keeping with its preference for misfolded proteins, CHIP appears to be particularly

important for turnover of destabilized LRRK2 variants, such as the sporadic PD risk allele LRRK2 G2385R, and may not be as relevant for WT or Mendelian LRRK2 PD mutants [85].

Results

TRIM1 ubiquitinates LRRK2 to regulate its turnover via the proteasome

Many TRIM family members are functional E3 ligases; however, it has not been conclusively determined if TRIM1's RING domain if enzymatically active. In order to determine if TRIM1 ubiquitinates LRRK2, we co-expressed Myc-TRIM1, FLAG-LRRK2, and HA-ubiquitin in HEK-293T cells. We then immunoprecipitated LRRK2 from the cell lysates and immunoblotted for ubiquitin. We found that LRRK2 co-immunoprecipitated with significantly more ubiquitin when TRIM1 was co-expressed, compared to a control vector (Figure 3.1A). Furthermore, we found TRIM1 expression led a higher degree of LRRK2 ubiquitination than CHIP expression, indicating that TRIM1 causes LRRK2 ubiquitination to a greater degree than a previously identified LRRK2-associated E3 ligase (Figure 3.1A).

We noted that lysate levels of LRRK2 were consistently lower when TRIM1 was co-expressed in cells. To interrogate this observation further, we transfected HEK-293T cells with LRRK2 and either Myc-TRIM1 or a control vector and collected cells for immunoblot analysis every 4-16 hours for 48 hours. We observed that LRRK2 levels were again consistently lower in the presence of Myc-TRIM1 (Figure 3.1B). To determine if this held true for endogenous protein, we knocked down TRIM1 mRNA in Malme-3M cells, which express relatively high levels of both LRRK2 and TRIM1 compared to other cell lines. siRNA against TRIM1 knocked

down TRIM1 mRNA levels to 33% +/- 6% (mean +/- standard deviation) relative to siRNA scrambled control (Figure 3.1C). Cells with TRIM1 knocked down had significantly higher levels of endogenous LRRK2 detected by immunoblot (162% +/- 13%, mean +/- standard deviation) 48 hours after knockdown (Figure 3.1D, quantified in Figure 3.1E).
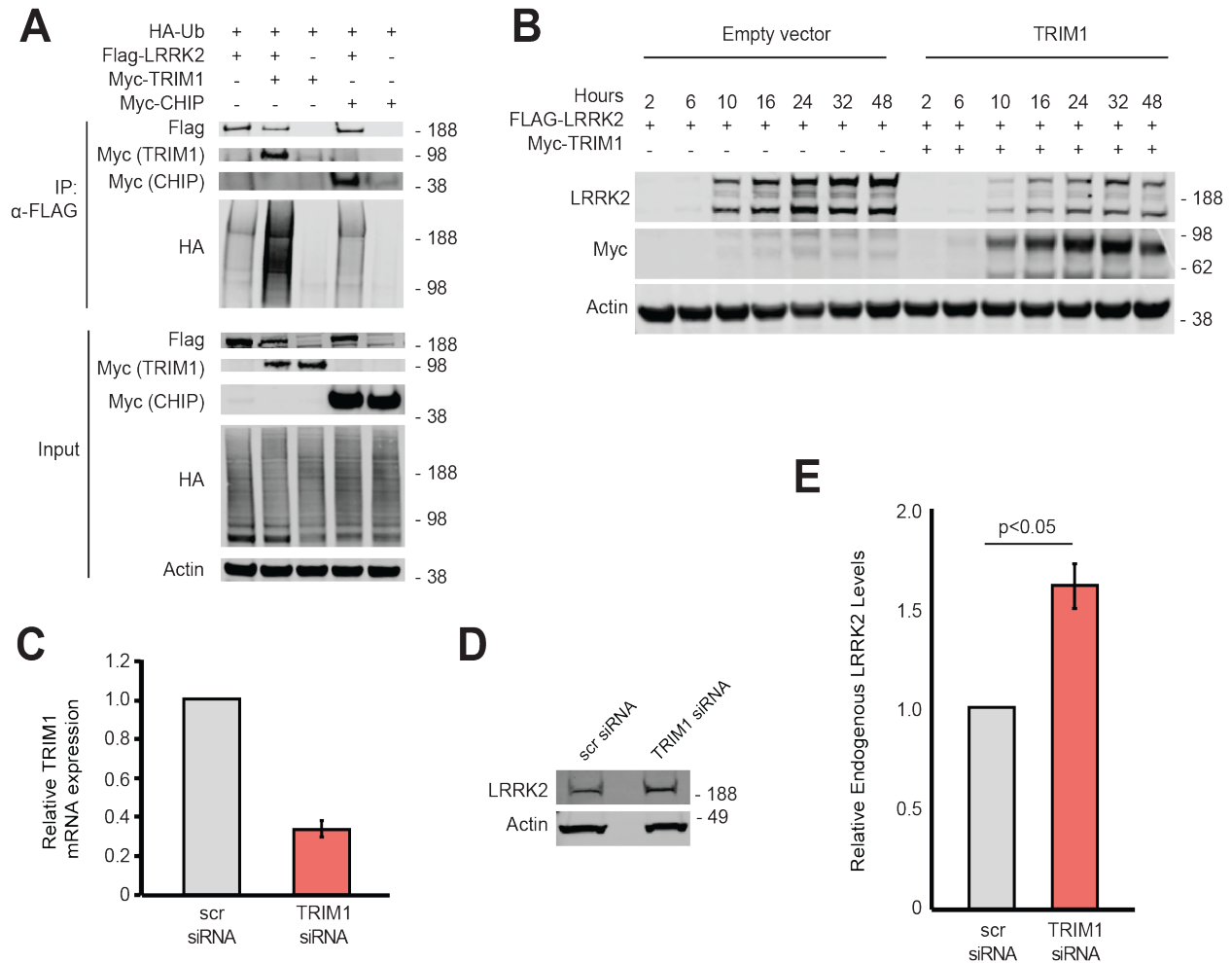
Figure 3.1. TRIM1 expression leads to ubiquitination and a decrease in LRRK2 protein levels. (A) Co-immunoprecipitation and ubiquitination of FLAG-LRRK2 with myc-TRIM1 or myc-CHIP in the presence of HA-ubiquitin in HEK-293T cells. (B) Immunoblot of FLAG-LRRK2 co-transfected with myc-TRIM1 or empty vector control. Time indicates hours after transfection. (C) Relative TRIM1 mRNA expression in Malme-3M cells with either scrambled siRNA (grey bar) or TRIM1-targeting siRNA (red bar). (D) Immunoblot of endogenous LRRK2 in lysates of Malme-3M cells with scrambled siRNA (left lane) or endogenous TRIM1 knocked down by targeted siRNA (right lane). (E) Quantification of (D) showing mean value from three separate experiments.

Although ubiquitination and decreased protein levels led us to believe TRIM1 might be causing LRRK2 to be degraded, we didn't have enough flexibility with immunoblotting systems to thoroughly investigate the process. We were concerned that, especially with over-expression, a significant portion of LRRK2 could be bound to microtubules and insoluble with co-expression of TRIM1, and thus not showing up in lysates. Additionally, it was difficult to fine-tune both timing and dosage of LRRK2 and TRIM1 expression. To address these concerns, we sought to develop a flow cytometric assay to measure LRRK2 protein levels inside living cells. For this assay, we utilized HEK-293T cells with a doxycycline ("dox")-inducible GFP-LRRK2 transgene (similar lines contained only GFP or GFP-LRRK2 PD mutants) [42]. To measure LRRK2 levels, GFP-LRRK2 expression was induced; cells were then transfected, had doxycycline removed, and/or were treated, depending on the experiment; and GFP fluorescence measured by flow cytometry (Figure 3.2A). We first verified that normalized median GFP fluorescence intensity of GFP-LRRK2 was indeed proportional to LRRK2 levels on immunoblot with no transfection or treatments (Figure 3.2B). Furthermore, we verified that TRIM1 had no effect on dox-GFP levels, indicating that any TRIM1 effects we saw in the dox-inducible LRRK2 lines were, in fact, LRRK2-specific (Figure 3.2C).

Using this novel assay, we measured LRRK2 protein levels *in vivo* with and without TRIM1 transfection. As anticipated based on the ubiquitination results, TRIM1 expression did lead to LRRK2 turnover (Figure 3.3A, quantified in Figure 3.3B). We additionally confirmed that the decrease in LRRK2 levels is dependent on TRIM1's E3 ligase activity by transfecting cells with TRIM1ΔRF, a TRIM1 construct lacking the enzymatic ring finger domain. Co-expression of ΔRF-TRIM1 caused no observable drop in LRRK2 levels compared to a control empty vector (Figure 3.3B).
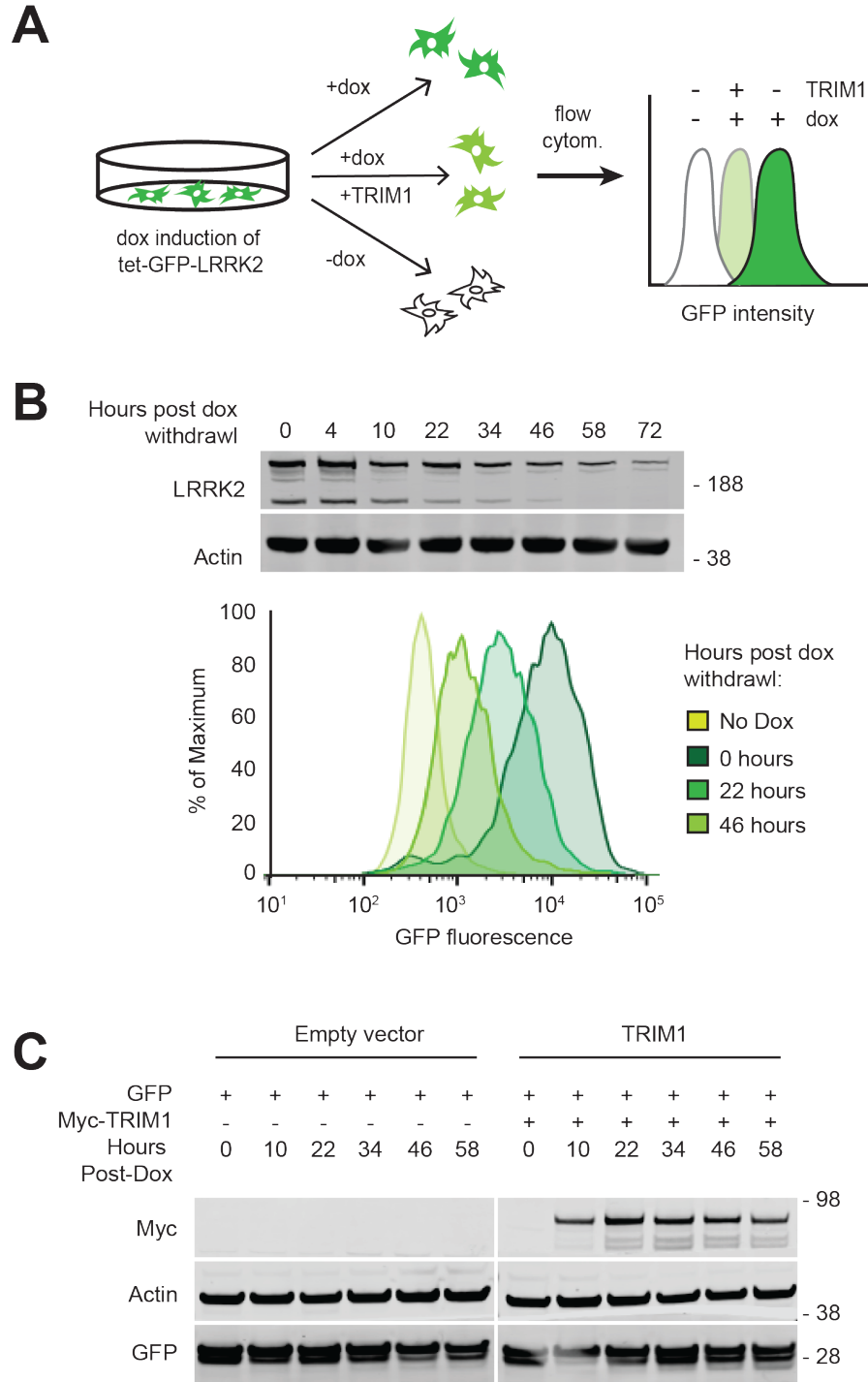
Figure 3.2. Flow cytometric assay to measure LRRK2 levels in cells. (A) Schematic of flow cytometric assay using fluorescence to measure GFP-LRRK2 turnover. Doxycycline-inducible GFP-LRRK2 HEK-293T cells are induced for 18 to 24 hours, transfected and doxycycline simultaneously withdrawn, and GFP fluorescence measured generally 24 hours later. (B) Immunoblot showing LRRK2 levels relative to actin after withdrawal of doxycycline (doxycycline-induced for 18 hours) and flow cyotmetric histograms of median GFP fluorescence from the same samples. (C) Immunoblot of dox-induced GFP expression transfected with myc-TRIM1 or empty vector control. Time indicates hours after transfection.

Because LRRK2 has been associated with both the autophagic-lysosomal and ubiquitin-proteasomal degradation pathways, we wanted to determine which pathway(s) led to TRIM1-dependent LRRK2 turnover. In our dox-LRRK2 system, we measured LRRK2 turnover with transient TRIM1 expression over 24 hours in the presence of 25 μM chloroquine (an autophagy inhibitory), 2 μM MG132 (a broad proteasomal inhibitor), or a DMSO vehicle. We found that MG132 fully blocked TRIM1-dependent turnover, while chloroquine treatment had no significant effect compared to vehicle (Figure 3.3C). Thus, we concluded that TRIM1 drives LRRK2 turnover via the proteasome.

Finally, we used this system to assess the effect of TRIM1 knockdown on LRRK2 over time. Using CRISPRi with catalytically dead Cas9 (dCas9) [86], we knocked down endogenous TRIM1 (Figure 3.3D). Because there is not much endogenous TRIM1 in HEK-293T cells, we did not want to overwhelm the system with huge amounts of LRRK2 protein, so we induced LRRK2 at low levels (2 ng/mL doxycycline instead of the typical 5ng/mL) for 24 hours, and measured GFP fluorescence after doxycycline withdrawal for 44 hours. We found a significant increase in LRRK2 levels in cells with TRIM1 knocked down compared to cells with control sgRNA (Figure 3.3E). This increase in GFP-LRRK2 protein levels was significant throughout the length of the experiment, and the relative amount of GFP-LRRK2 protein present in the cells with TRIM1 sgRNA increased over time, indicating a persistent LRRK2 turnover deficit in these cells. Together, these data indicate that TRIM1 ubiquitinates LRRK2, leading to LRRK2 degradation via the proteasome, and that endogenous TRIM1 is important for maintaining LRRK2 protein levels in cells.
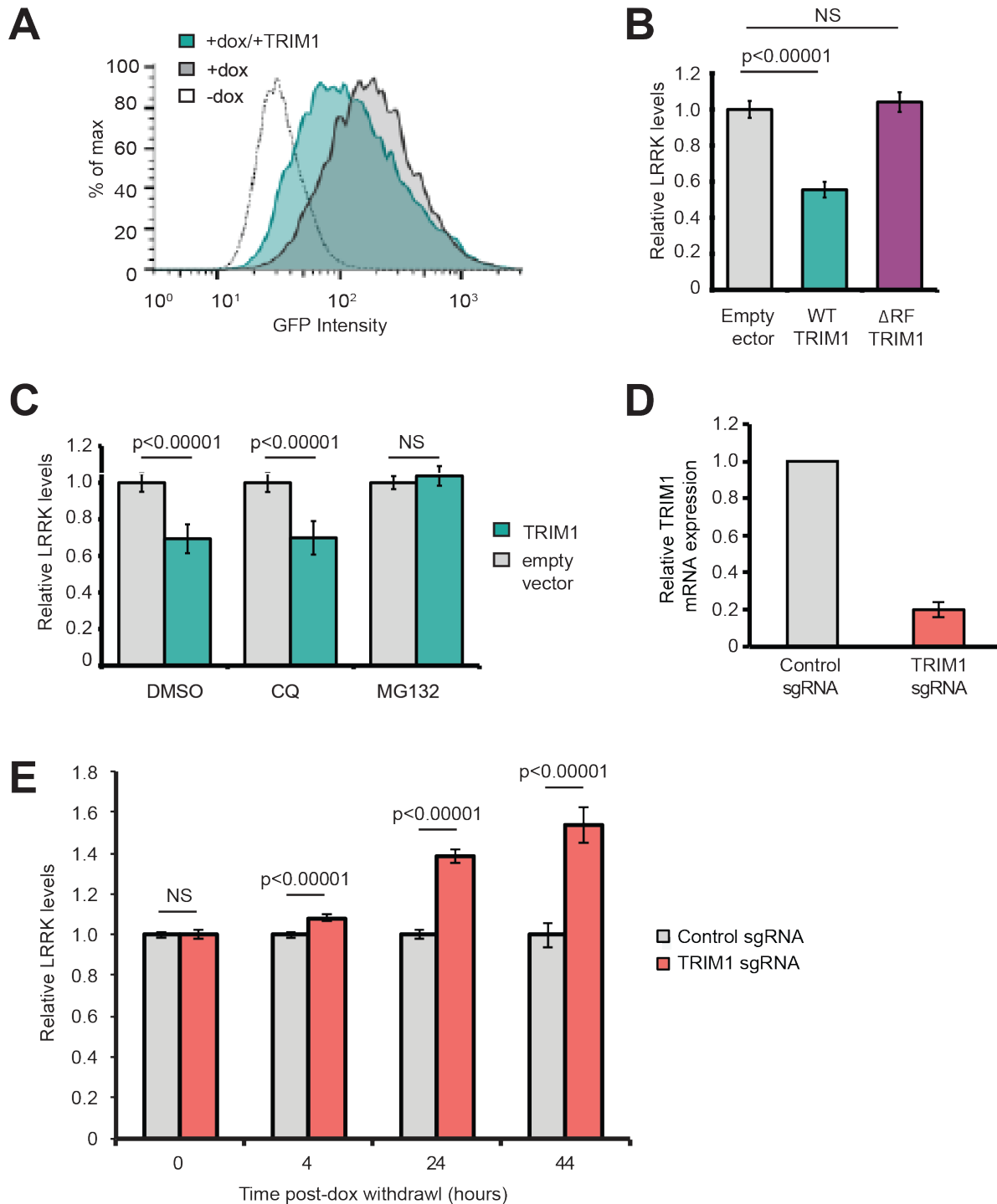
Figure 3.3. TRIM1 drives LRRK2 proteasomal turnover. **(A)** Representative histograms of GFP-LRRK2 fluorescence in the absence or presence of doxycycline followed by TRIM1 or empty vector transfection. **(B)** Quantification of GFP-LRRK2 levels 24 hours after doxycycline withdrawal in the presence of empty vector (grey bar), TRIM1 (teal bar), and ring-finger deleted (ΔRF) TRIM1 (purple bar). **(C)** Quantification of GFP-LRRK2 levels in the presence of chloroquine at 25 μM for 24 hours (CQ), MG132 at 2 μM for 24 hours, or equivalent volume of DMSO vehicle. **(D)** Relative TRIM1 mRNA expression in dox-inducible GFP-LRRK2 HEK-293T cells with dCas9 and either non-targeting sgRNA (grey bar) or four pooled TRIM1-targeting sgRNAs (red bar). **(E)** Flow cytometric quantification of GFP-LRRK2 levels in TRIM1 knockdown and control lines at 0, 4, 24, and 44 hours after doxycycline withdrawal relative to control cells at all time points.

TRIM1 inhibits LRRK2 kinase activation by Rab29

Rab29, which is localized to Golgi network membranes, was recently identified as an activator of LRRK2 kinase function. Over-expression of Rab29 leads to increased LRRK2 kinase activity, measured by auto-phosphorylation at Ser1292, phosphorylation of Rab29 at Thr71, and phosphorylation of Rab10 at Thr73 [43]. Additionally, activation is measurably stronger with GTPase-domain LRRK2-PD mutants such as LRRK2 R1441G. To assess whether TRIM1 had any effect on Rab29-mediated activation of LRRK2, we co-expressed wild type LRRK2 or LRRK2 R1441G with Myc-TRIM1 and/or HA-Rab29. We confirmed previous reports that Rab29 expression leads to increased LRRK2 Ser1292 auto-phosphorylation, and that this effect is even greater for LRRK2 R1441G than WT (Figure 3.4A, quantified in Figure 3.4B). Expressing TRIM1 with LRRK2 alone had no effect on Ser1292 phosphorylation, but when TRIM1 was expressed with Rab29, Ser1292 phosphorylation levels were decreased back to near baseline levels of phosphorylation observed in the absence of Rab29 over-expression (Figure 3.4A, 3.4B). Furthermore, we measured Rab29 phosphorylation at Thr71 and Rab10 phosphorylation at Thr73 as a measure of LRRK2 kinase activity beyond auto-phosphorylation. Co-expression of TRIM1 led to a significant decrease in Rab29 and Rab10 phosphorylation (Figure 3.4A, quantified in Figures 3.4C and 3.4D). Together, these data suggest that TRIM1 inhibits Rab29's ability to activate LRRK2's kinase function.

To begin to dissect the mechanism by which TRIM1 inhibits Rab29-mediated LRRK2 activation, we utilized two TRIM1 variants: TRIM1ΔRF and TRIM1 C. TRIM1ΔRF is missing its N-terminal ring finger domain, and therefore lacks E3 ligase activity, but maintains its microtubule localization. TRIM1 C has six mutated amino acids in its C-terminal COS box domain (FLQ328AAA LDY377AAA) [69], abolishing its ability to bind microtubules (Figure

3.5A), but maintaining its E3 ligase function (Figure 3.5B). By expressing these TRIM1 variants with Rab29 and WT LRRK or LRRK2 R1441G, we found that, identical to WT TRIM1, TRIM1 C inhibits Rab29-mediated LRRK2 activation, as measured by Rab29 T71 phosphorylation (Figure 3.5C, quantified in Figure 3.5D). Intriguingly, TRIM1ΔRF does not inhibit Rab29-mediated LRRK2 activation, suggesting that TRIM1's E3 ubiquitin ligase function is required for its role in regulating LRRK2 activation.
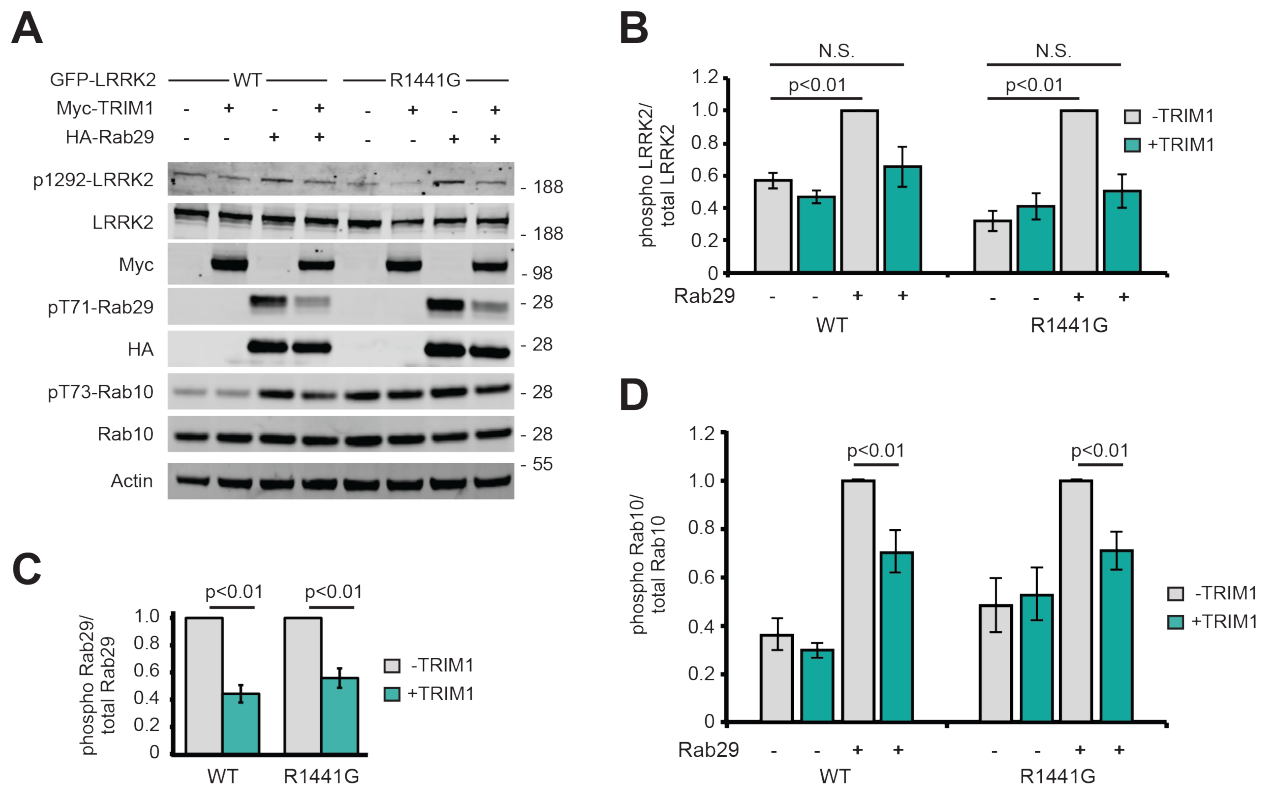
Figure 3.4. TRIM1 inhibits Rab29-mediated LRRK2 activation. (A) Immunoblot of LRRK2 phosphorylation at Ser1292, Rab29 phosphorylation at Thr71, and Rab10 phosphorylation at Thr73 in the presence and absence of TRIM1 for wild type LRRK2 and LRRK2-PD mutant R1441G. (B) Quantification of LRRK2 auto-phosphorylation in (A). (C) Quantification of Rab29 Thr71 phosphorylation in (A). (D) Quantification of Rab10 Thr73 phosphorylation in (A). All immunoblots are representative images and quantification shows the mean value from three separate experiments.
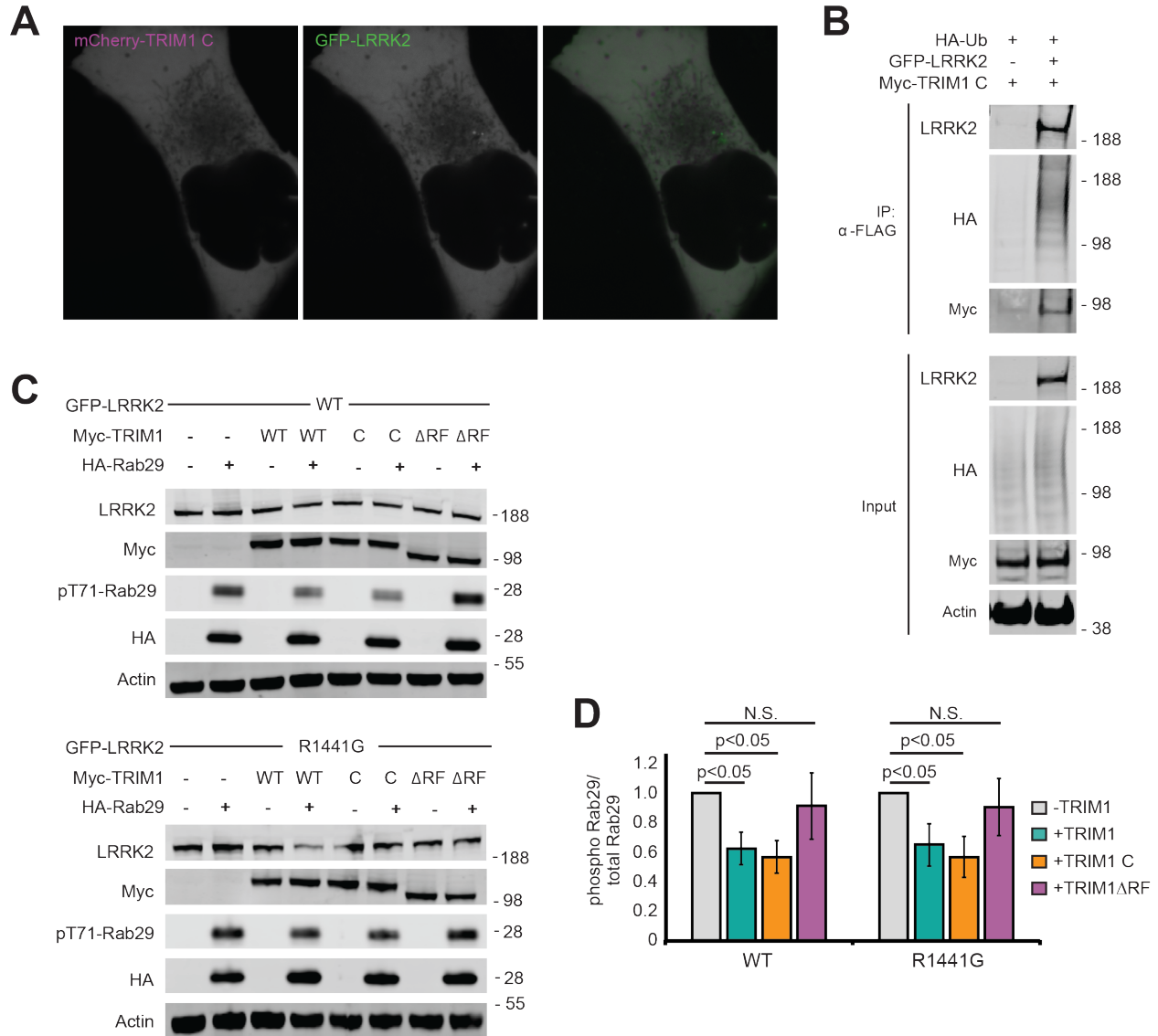
Figure 3.5. TRIM1's affect on Rab29-mediated LRRK2 activation is E3 ubiquitin ligase-dependent. (A) Live-cell confocal microscopy of GFP-LRRK2 and mCherry-TRIM1 C transiently transfected into H1299 cells. From left to right, mCherry-TRIM1 C, GFP-LRRK2, merged image. (B) Co-immunoprecipitation and ubiquitination of GFP-LRRK2 with myc-TRIM1 C in the presence of HA-ubiquitin in HEK-293T cells. (C) Immunoblot of Rab29 phosphorylation with WT LRRK2 and LRRK2 R1441C in the absence of TRIM1 or with over-expression of myc-tagged wild type TRIM1, microtubule-nonbinding TRIM1 (TRIM1 C), or TRIM1 lacking E3-ligase function (TRIM1ΔRF). (D) Quantification of Rab29 phosphorylation in (C).

TRIM1 rescues the neurite outgrowth defect caused by LRRK2 G2019S

Of the LRRK2 PD-driving point mutations, the most common is LRRK2 G2019S, which causes deficiencies in neurite outgrowth, a microtubule-driven process thought to reflect neuronal health [41, 44]. Similar to WT LRRK2, LRRK2 G2019S co-localizes with microtubules (Figure 3.6A), gets ubiquitinated (Figure 3.6B), and is degraded via the proteasome (Figure 3.6C) in a TRIM1-dependent manner. To test the ability of TRIM1 to restore neurite outgrowth deficiencies caused by expression of LRRK2 G2019S, we used a previously published rat PC12 pheochromocytoma cell line harboring dox-inducible LRRK2 G2019S [87]. These cells were transfected with mCherry-TRIM1 or control vector, doxycycline-induced, and treated with nerve growth factor (NGF) for 4 days to induce neurite outgrowth. The proportion of cells with neurites (defined as cellular process greater than cell body length) [88] was quantified. Expression of TRIM1 alone did not affect PC12 neurite outgrowth (49% +/- 2% neurite-bearing cells without TRIM1; 46% +/- 9% neurite-bearing cells with TRIM1, p =0.65) (Figure 3.6D, quantified in Figure 3.6E). LRRK2 G2019S expression, however, significantly reduced outgrowth, a phenotype that was completely rescued by co-expression of TRIM1 (29% +/- 6% neurite-bearing cells without TRIM1; 44% +/- 6% neurite-bearing cells with TRIM1; p =0.03) (Figure 3.6D, quantified in Figure 3.6E). These results suggest a new model for regulation of LRRK2 in which the phosphorylation status of key serine residues in its RL determines its choice of binding partner (14-3-3 vs. TRIM1), cellular location (cytoplasm vs. microtubule), ubiquitination and proteasomal degradation, Rab29-dependent kinase activation, and, in the case of mutant LRRK2 G2019S, its neurotoxicity (Figure 3.6F).

Figure 3.6. TRIM1 mediates proteasomal degradation of PD-mutant LRRK2 G2019S to rescue its toxicity.
(A) Live-cell confocal microscopy of GFP-LRRK2 G2019S and mcherry-TRIM1 transiently transfected into H1299 cells. From left to right: mCherry-TRIM1, GFP-LRRK2, merged image. Inset shows higher magnification of region identified by box in merged image. (B) Co-immunoprecipitation and ubiquitination of

(Figure 3.6, continued) GFP-LRRK2 G2019S with myc-TRIM1 in the presence of HA-ubiquitin in HEK-293T cells. (C) Flow cytometric analysis of dox-inducible GFP-LRRK2 G2019S HEK-293T cells in the presence and absence of TRIM1 and the proteasome inhibitor MG132 or vehicle; bars show median green fluorescence intensity with error bars showing twice the standard error of the mean. (D) Representative dox-inducible LRRK2 G2019S PC-12 cells transfected with mCherry-TRIM1 or mCherry alone vector and GFP and differentiated with NGF for 5 days in the presence and absence of 1 mg/mL doxycycline. (E) Quantification of the fraction of neurite-bearing PC-12 cells; bars show average of three separate experiments of 150-250 cells each, error bars show standard error of the mean. (F) Model of the TRIM1/LRRK2 interaction highlighting the role of the RL in determining binding partners, localization, ubiquitination, proteasomal degradation, kinase activity, and toxicity.

Discussion

We found that TRIM1 ubiquitinates LRRK2 and targets it for degradation by the proteasome. We observed LRRK2 turnover by immunoblot, as well as in live cells by flow cytometry. We also observed that knockdown of endogenous TRIM1 is sufficient to increase endogenous LRRK2 protein levels in cells. While this process *in vivo* likely occurs at the microtubule, as shown in Chapter II, we don't believe that microtubule localization is essential for LRRK2 turnover, as evidenced by our characterization of mutant TRIM1 C. Prior to this work, CHIP was the only E3 ligase known to ubiquitinate LRRK2 leading to proteasomal degradation. Notably, in the same assay, we found that TRIM1 ubiquitinates LRRK2 to a greater extent than CHIP. TRIM1, a RING finger E3 ligase, and CHIP, a Ubox E3 ligase, are different classes of E3 ligases, and they bind LRRK2 in different regions: TRIM1 binds the unstructured regulatory loop between the Ankyrin and LRR domains, while CHIP binds the Roc domain in LRRK2's catalytic core [84].

Our data also show that TRIM1 can decrease Rab29-mediated LRRK2 activation *in vivo*, both for WT and a PD mutant form of LRRK2, highlighting its potential significance as a clinical target. Adding to this, we observed that TRIM1 is able to rescue LRRK2 G2019S-driven

deficits in neurite outgrowth, a common measure of PD-related cytotoxicity. Fitting with the theory that LRRK2 protein levels are an important determinant of LRRK2-driven cytotoxicity, we see that the ability of TRIM1 to ubiquitinate LRRK2 is essential for TRIM1's inhibition of LRRK2 kinase activation by Rab29. As a future step, it would be beneficial to examine neurite outgrowth in the presence of TRIM1 C and TRIM1ΔRF to determine whether or not TRIM1's ameliorative role in this process is microtubule- and/or E3 ligase-dependent.

Intriguingly, while PD-causing mutations in LRRK2 are associated with protein accumulation and impaired turnover [51], LRRK2 mutations that increase risk for Crohn's disease and leprosy cause decreased protein stability and abundance [26, 27]. This suggests that there is a fine line between too much and too little LRRK2, and that disrupting this balance may lead to different disease phenotypes in different tissues. It would be interesting in future work to examine the interaction between TRIM1 and Crohn's/leprosy mutant LRRK2, and to determine if TRIM1-mediated LRRK2 turnover plays an important in these other conditions, as well.

CHAPTER IV: IDENTIFICATION OF LRRK2 TURNOVER REGULATORS DOWNSTREAM OF KINASE INHIBITION

Introduction

Just one year after it was identified as the gene in the PARK8 locus responsible for familial PD cases, LRRK2 mutations were linked to increased kinase activity [49]. This was shown first with *in vitro* kinase assays, and later confirmed with *in vivo* analysis of LRRK2 auto-phosphorylation [41] and Rab phosphorylation [39]. This finding indicated that LRRK2 could be a druggable target as a kinase with what appears to be a gain-of-function mutation, a rare find in neurodegenerative disorders [89]. Early studies proved that LRRK2 could be inhibited with small molecules *in vitro*, and by 2011, a number of first generation selective LRRK2 inhibitors, including LRRK2-IN-1, were identified [90]. In 2015, work on MLi-2, a third generation inhibitor with greatly improved potency, was published [91]. However, excitement around LRRK2 kinase inhibitors was somewhat quelled when GNE7915 and other inhibitors were tested in non-human primates and caused an aberrant accumulation of lamellar bodies in type II pneumocytes in the primates' lungs, indicating a defect in secretion or lysosomal function in these cells [92]. This same effect was seen in the lungs of mice treated with MLi-2 [91]. Importantly, the lung phenotype seen after LRRK2 kinase inhibition phenocopies pathology seen in LRRK2 knockout rats [59], suggesting that this is the direct consequence of LRRK2 inhibition, rather than an off-target effect of the inhibitors.

Follow up investigations on LRRK2 kinase inhibitors sought to better understand their effect on LRRK2, in hopes of finding a way to achieve neuroprotection without the deleterious

effects observed in peripheral organs. It was found that kinase inhibition leads to dephosphorylation of several serines in the LRRK2 Regulatory Loop (Ser910, Ser935, Ser955, and Ser973) [42]. Dephosphorylation leads to rapid ubiquitination and proteasomal degradation of LRRK2. This is observed in over-expression systems for WT and G2019S LRRK2, as well as with endogenous LRRK2 in brain, lung, and kidney tissues in mice [83]. These findings may indicate why LRRK2 kinase inhibition has a similar phenotype to LRRK2 knockout – in addition to affecting the kinase activity, LRRK2 expression itself is largely decreased. Interestingly, synthetic kinase-dead forms of LRRK2 are unstable and are also rapidly degraded *in vivo* [30], making the interplay between kinase activity and LRRK2 protein levels difficult to untangle. Adding to the complexity, recent work has found that total LRRK2 protein levels, rather than kinase activity, are important for LRRK2-driven neuronal toxicity [50]. This also fits with data that show LRRK2 G2019S is turned over more slowly and is present at higher steady-state levels than WT LRRK2 [51]. Thus, it is possible that LRRK2's kinase-independent functions, possibly as a protein scaffold, could be targets for PD therapeutics. Alternatively, maybe it is important to maintain LRRK2 protein levels for peripheral homeostasis while inhibiting LRRK2's kinase activity.

Interestingly, this phenomenon has been observed with other kinases and small molecule inhibitors, mostly in the context of cancer therapeutics. For example, kinase inhibitors for HER2, mutant EGFR, mutant B-Raf, and TRIB2 (a pseudokinase) can all cause protein instability and proteasomal degradation of their targets [93-95]. In general, this is seen as a clinical benefit: by eliminating not only kinase function, but also the kinase-independent roles of these oncogenic proteins, inhibitor-induced degradation can prevent the emergence of some cases of drug resistance [96, 97]. However, unlike in cancers, it is unclear whether maintaining

LRRK2 kinase function, protein levels, or possibly neither would be most beneficial in PD cases. By further understanding LRRK2 turnover, specifically downstream of kinase inhibitors, we may be able to better understand the relationship between LRRK2 kinase activity and LRRK2 protein abundance, and how to independently tune the two in potential PD treatments.

Results

LRRK2 is ubiquitinated by an unknown E3 ligase and degraded following kinase inhibition

We confirmed previous reports that LRRK2 kinase inhibition leads to LRRK2 degradation [42, 83]. In our dox-inducible GFP-LRRK2 cells, we found that treatment with 100 nM MLi-2 led to a 58.7% +/- 10.3% decrease in LRRK2 levels after 18 hours, compared to vehicle-treated cells (Figure 4.1A, quantified in Figure 4.1B). While endogenous LRRK2 is generally hard to detect, we also found that MLi-2 treatment (500 nM for 48 hours) led to a 22.2% +/- 11.4% decrease in endogenous LRRK2 levels in BV2 cells (Figure 4.1C, quantified in Figure 4.1D). We also confirmed reports that inhibition leads to LRRK2 ubiquitination [42]. We immunoprecipitated GFP-LRRK2 from cells transiently transfected with HA-ubiquitin in the presence of MG132 to prevent degradation. We found LRRK2 was associated with significantly more HA-ubiquitin in cells treated with 100 nM MLi-2 than vehicle-treated cells (Figure 4.1E, quantified in Figure 4.1F).
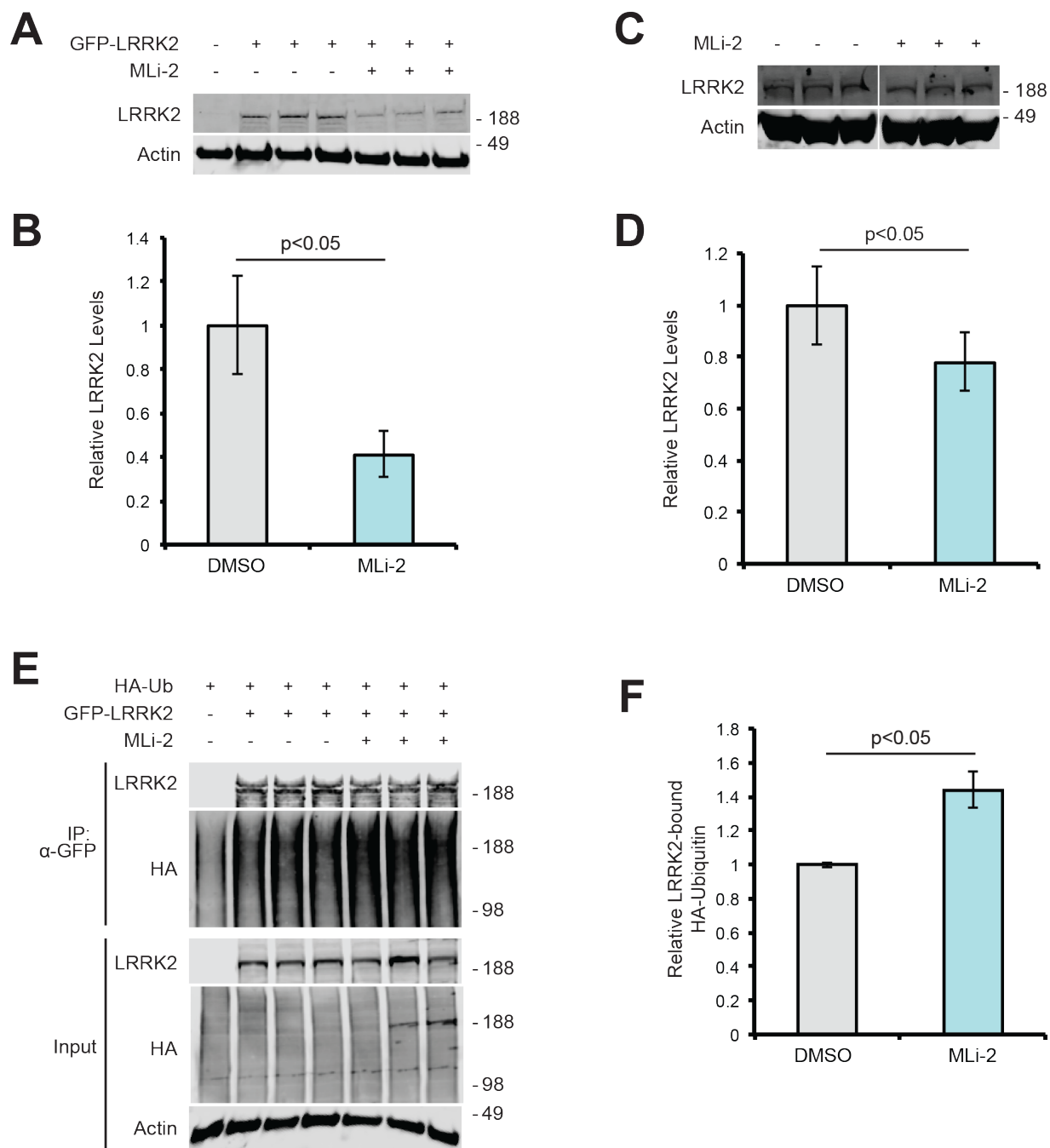
Figure 4.1. LRRK2 is ubiquitinated and turned over following kinase inhibition. (A) Immunoblot of GFP-LRRK2 from cells treated with 100 nM MLi-2 or vehicle for 18 hours following doxycycline withdrawal. (B) Quantification of LRRK2 levels relative to actin levels in (A). (C) Immunoblot of endogenous LRRK2 from BV2 cells treated with 500 nM MLi-2 or vehicle for 24 hours. (D) Quantification of LRRK2 levels in (C). (E) Co-immunoprecipitation of GFP-LRRK2 with HA-ubiquitin from cells treated with 2 μM MG132 and 100 nM MLi-2 or vehicle for 18 hours following doxycycline withdrawal. (F) Quantification of ubiquitin levels relative to LRRK2 levels in (E).

Using the flow cytometric assay introduced in Chapter III to track GFP-LRRK2 levels, we further confirmed that kinase inhibition leads to LRRK2 degradation by the proteasome, as MG132 mostly blocked a decrease in LRRK2 levels after MLi-2 treatment, while inhibiting autophagic turnover with chloroquine had little effect on LRRK2 levels relative to DMSO (Figure 4.2A). We further tested an array of LRRK2 kinase inhibitors, including first generation compounds developed at the Dana Farber Cancer Institute (LRRK2-IN-1) [98] and GlaxoSmithKline (GSK2578215A) [99]; second generation compounds from Genentech, G1023 [41] and GNE-7915 [100]; in addition to MLi-2, a third generation compound developed by Merck [91]. We found that all inhibitors tested, across generations, manufacturers, and chemical structures [41, 90, 101], caused LRRK2 turnover via the proteasome (Figure 4.2B, structures shown in Figure 4.2C), indicating that this is likely a universal effect of kinase inhibition on LRRK2, rather than an off-target effect of one compound.

There are three E3 ligases known to ubiquitinate LRRK2: CHIP [62, 84], WSB1 [61], and TRIM1 (see chapters II and III). Both CHIP and TRIM1 are additionally known to cause LRRK2 proteasomal degradation. To determine if any of these known LRRK2-associated E3 ligases are involved in ubiquitination and degradation following kinase inhibition, we utilized CRISPRi with our flow cytometric assay. We inserted a catalytically dead dCas9 transgene into our dox-inducible GFP-LRRK2 cell line, and then added sgRNA sequences targeted at our E3 ligases of interest (Figure 4.3A). dCas9 transcriptionally inactivates genes by binding to their 5' UTR region and inhibiting transcription (Figure 4.3B). We used 2-4 sgRNAs per gene to individually knockdown TRIM1, CHIP, and WSB1, as well as PSMC4, a proteasomal component used as a positive control for the assy. LRRK2 expression was induced for 24 hours with 5 ng/mL doxycycline, and then 100nM MLi-2 or vehicle was added to the cells for 24 hours

after doxycycline withdrawal. We found that knockdown of the known LRRK2-associated E3 ligases had no effect on LRRK2 levels after MLi-2 treatment (Figure 4.3C), indicating that there must be at least one additional E3 ubiquitin ligase that plays a critical role in regulating LRRK2 turnover in the context of kinase inhibition.
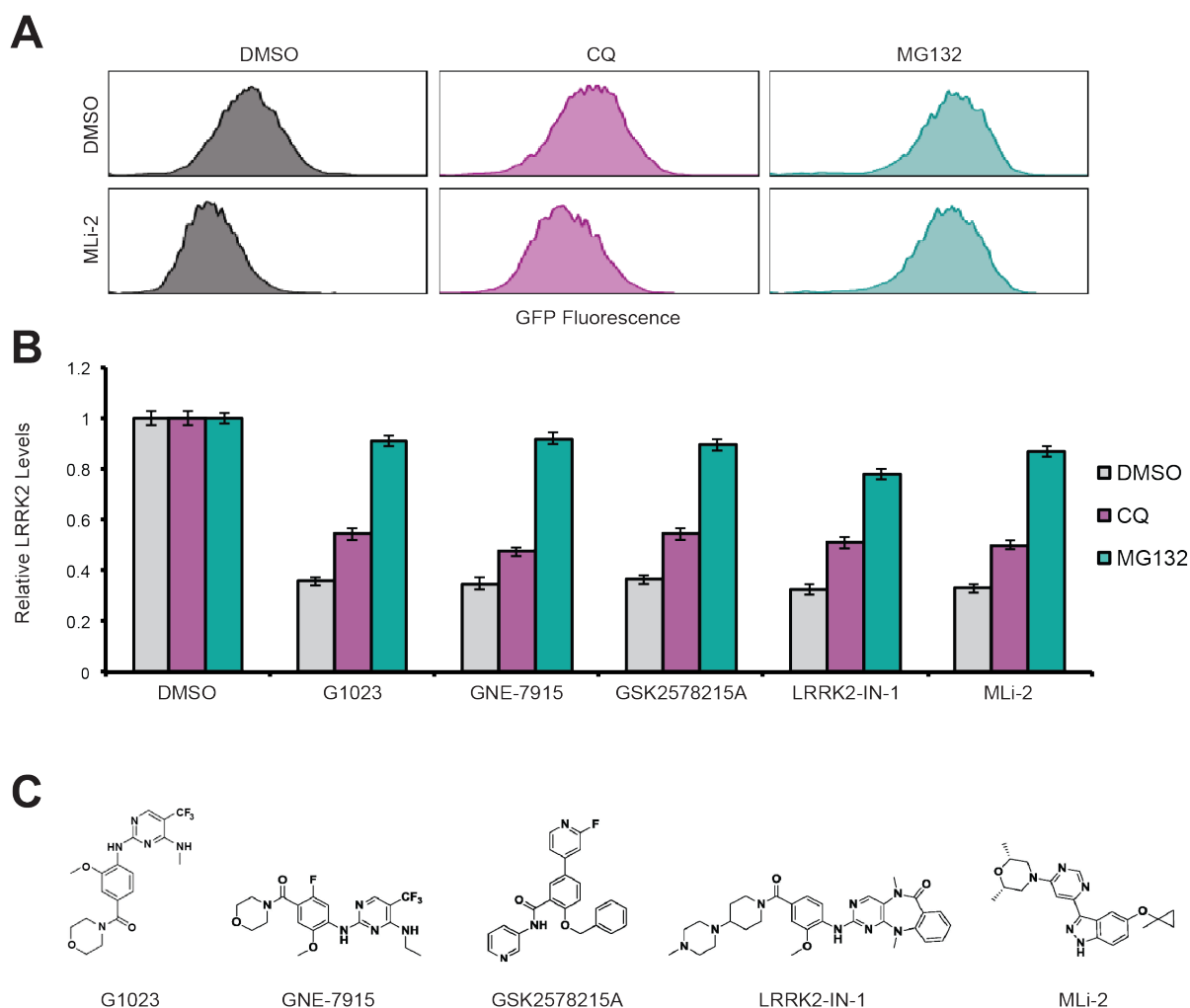
Figure 4.2. LRRK2 proteasomal degradation occurs across kinase inhibitors.   (A) Representative histograms of GFP-LRRK2 fluorescence after vehicle or 100 nM MLi-2 co-treatment with MG132 (2 μM) or chloroquine (25 μM) for 24 hours. (B) Quantification of GFP-LRRK2 levels 24 hours after doxycycline withdrawal in the presence of DMSO (grey bar), 25 μM chloroquine (purple bar), or 2 μM MG132 (purple bar). Cells were concurrently treated with LRRK2 kinase inhibitor indicated on the X-axis for 24 hours at 10 μM, except in the case of MLi-2, which was used at 100 nM. (C) Structures of LRRK2 kinase inhibitors used in (B).
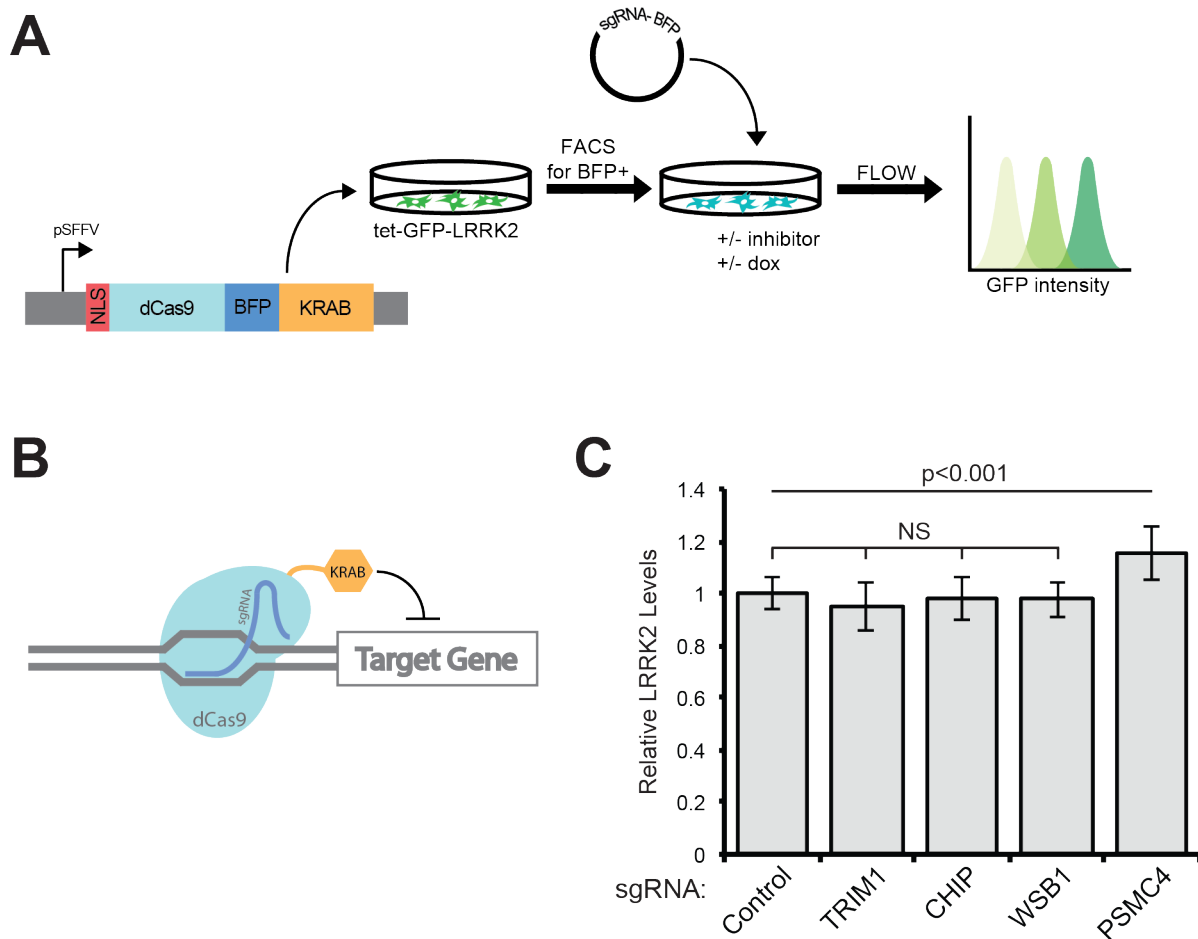
Figure 4.3. CRISPRi system indicates LRRK2 turnover is driven by an unknown E3 ligase. (A) Schematic of CRISPRi used with flow cytometric assay. dCas9-BFP with a Krüpple-Associated Box (KRAB) effector is inserted into doxycycline-inducible GFP-LRRK2 HEK-293T cells and cells are sorted for a BFP+ pure population. Single or multiple sgRNA plasmids are added to cells by lentivirus or transfection, and cells are induced and subsequently treated with LRRK2 kinases inhibitors or other compounds, and GFP fluorescence measured generally 24 hours later. (B) Schematic illustrating the mechanism of action of dCas9-KRAB in complex with a sgRNA. sgRNA oligos are complementary to the 5' UTR of genes of interest. dCas9 binds the promoter region, but does not cut the genome, and the KRAB effector additionally represses transcription. (C) Quantification of LRRK2 levels with TRIM1, CHIP, WSB1, or PSMC4 knocked down relative to a control sgRNA after 24 hours of 100 nM MLi-2 treatment, as measured by median GFP fluorescence. Only PSMC4, a component of the proteasome, significantly prevented LRRK2 degradation after kinase inhibition.

CRISPRi screen identifies novel regulators of LRRK2 turnover

Because no known LRRK2-associated E3 ligases appear to be important for LRRK2 ubiquitination and degradation following kinase inhibition, we opted to do a CRISPRi screen with a sgRNA library covering 3,093 stress and proteostasis genes, including nearly all of the

48

estimated 600-700 human E3 ubiquitin ligase genes [102]. Dox-inducible GFP-LRRK2 cells with dCas9-BFP were plated and infected in order to get at least 1,000-fold coverage per sgRNA (5 guides per gene). Following lentiviral infection with the sgRNA library and puromycin selection, cells were re-plated and doxycycline induced. After 24 hours, doxycycline was washed out and half of the cells were treated with 100 nM MLi-2, while the other half were given media with an equivalent volume of DMSO. 24 hours after treatment, unsorted cells were frozen and remaining cells were analyzed by flow cytometry. The top 10% of LRRK2-expressing cells (by GFP fluorescence) were collected for analysis (Figure 4.4A).

sgRNA oligos from sorted and unsorted frozen samples were prepared for sequencing. sgRNA sequences were counted for each sample and mapped to a sgRNA library to associate the counts with genes. We calculated two phenotype statistics: tau and gamma, corresponding to the fold enrichment in the sorted populations relative to unsorted for MLi-2-treated cells and vehicle-treated cells, respectively (Figure 4.4B). We focused on genes enriched in the sorted cell populations – i.e. genes that, when knocked down, lead to increased LRRK2 protein levels. 73 genes were significantly enriched in the DMSO sorted population ($p < 0.05$, gamma > 0; Figure 4.5 and top hits in Table 4.1). 76 genes were significantly enriched in the MLi-2 sorted population ($p < 0.05$, tau >0; Figure 4.6 and top hits in Table 4.2). Represented in both groups were members of the DnaJ HSP40 family of co-chaperones (DNAJA2, DNAJB12, and DNAJC5B for gamma; DNAJA3, DNAJC12, and DNAJC28 for tau), F-Box-containing substrate recognition components of SCF E3 ubiquitin ligase complexes (FBXO21 and FBXW5 for gamma, and FBXL3 for tau), and vacuolar protein sorting family members involved in vesicular trafficking and lysosomal degradation (VPS16 for gamma, and VPS13A and VPS35 for tau). Furthermore, several TRIM family members were significantly enriched in one of the

two populations, including TRIM21, TRIM46, and TRIM77. Some expected targets were significantly enriched, such as proteasomal assembly protein PSMD10 (gamma = 1.04), CHIP (gamma = 2.41), and ubiquitin D (gamma = 5.49).

A

B

$$tau = \log_2 \frac{\text{sgRNA count in MLi-2, sorted}}{\text{sgRNA count in MLi-2, unsorted}}$$

$$gamma = \log_2 \frac{\text{sgRNA count in DMSO, sorted}}{\text{sgRNA count in DMSO, unsorted}}$$
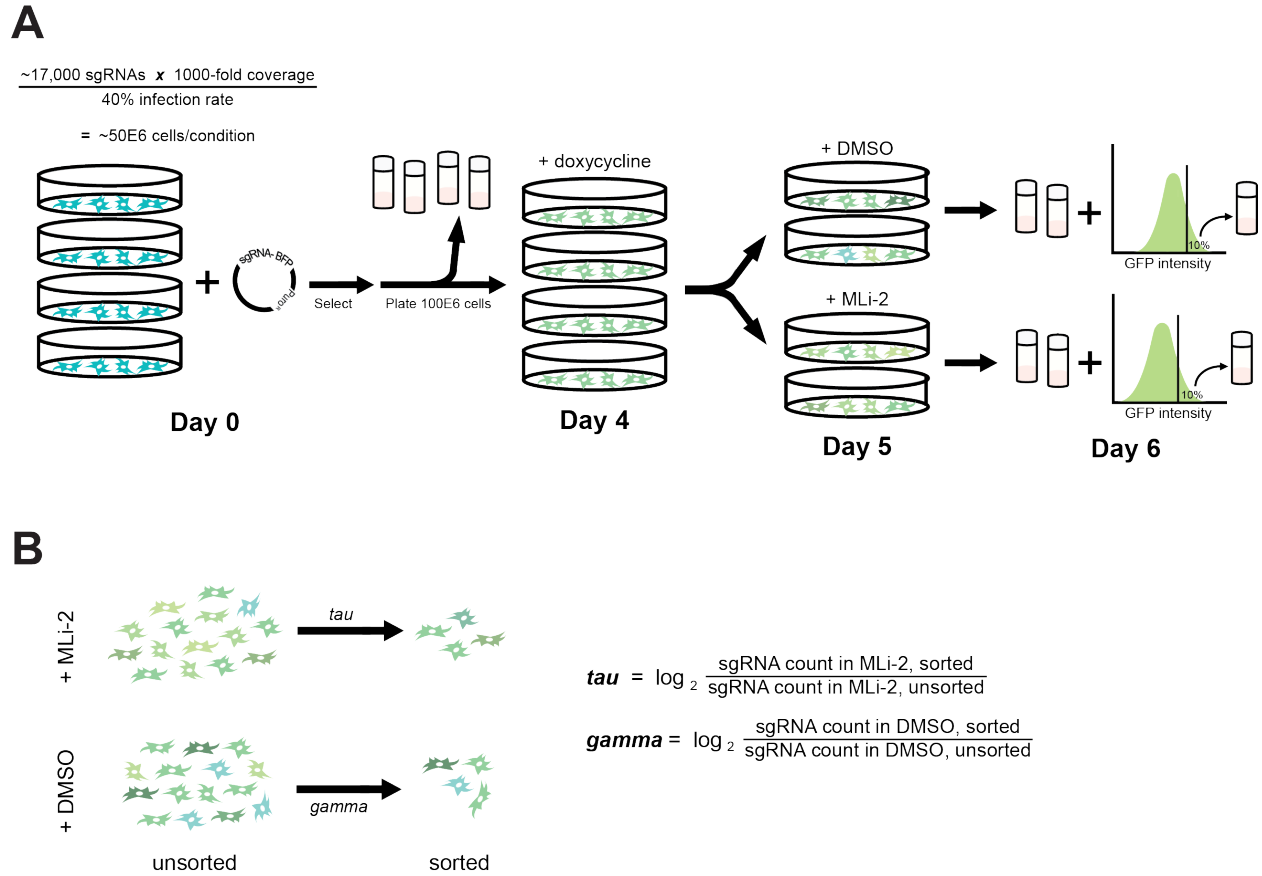
Figure 4.4. CRISPRi screen to identify regulators of LRRK2 turnover. (A) Schematic of CRISPRi screen procedure. Dox-inducible GFP-LRRK2 cells with dCas9-BFP were infected with lentiviral particles containing nearly 17,000 unique BFP-sgRNA oligos. Cells were doxycycline-induced and treated with 100 nM MLi-2 or vehicle and then sorted. Final sorted population was frozen for analysis, as were unsorted populations and baseline samples from before induction and treatment. (B) Schematic of two phenotype statistics, gamma and tau. Gamma corresponds to the enrichment of sgRNAs for a particular gene in the sorted, DMSO-treated population relative to the unsorted, DMSO-treated population. Tau corresponds to the enrichment of sgRNAs for a particular gene in the sorted, MLi-2-treated population relative to the unsorted, MLi-2-treated population.
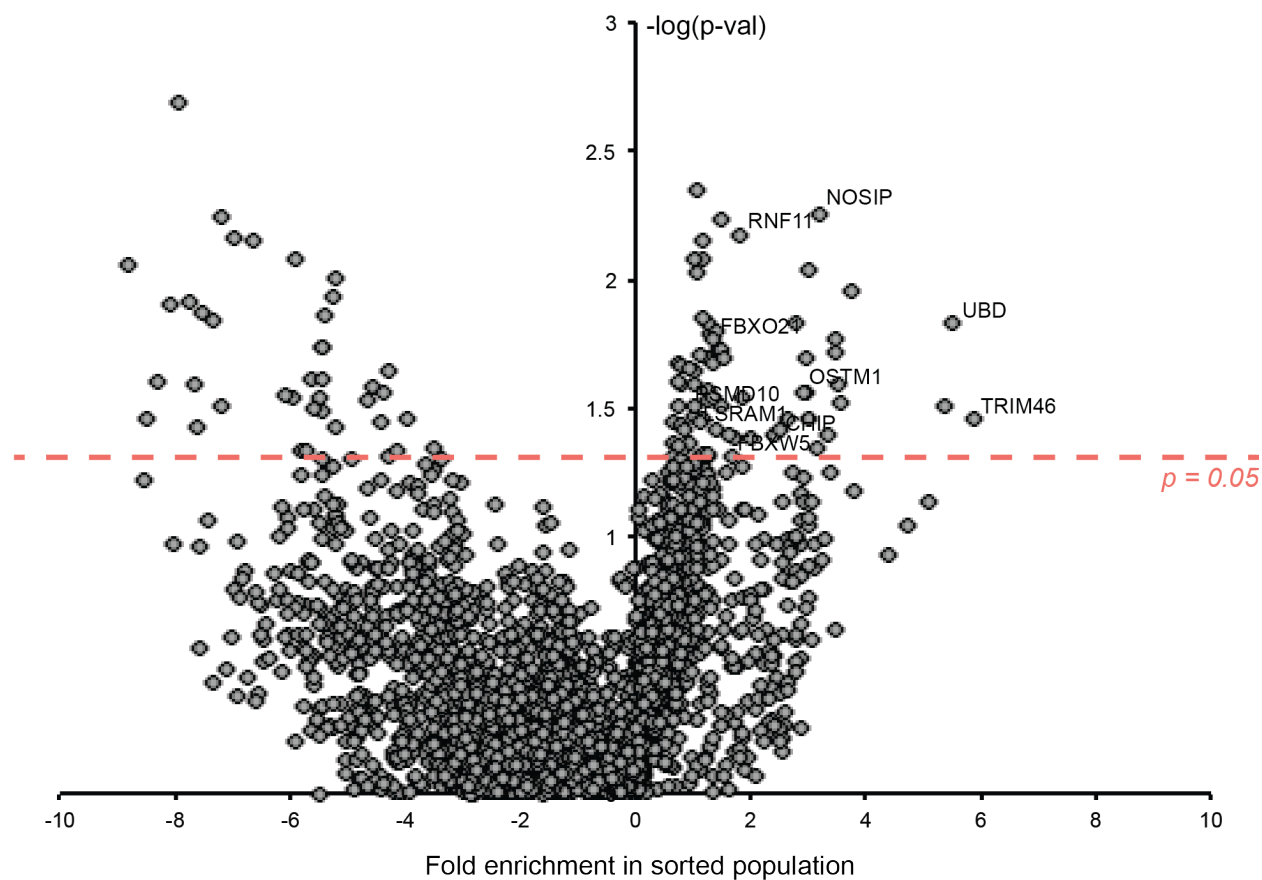
Figure 4.5. Genes involved in kinase inhibitor-independent LRRK2 turnover. Volcano plot of 3,093 stress and proteostasis genes showing negative log of p-values vs. their sgRNA enrichment in sorted population relative to unsorted population for vehicle-treated cells (gamma). Significance is defined as $p < 0.05$, indicated by the red dashed line. Notable genes are labeled (see Table 4.1 for details).

Table 4.1. Enriched genes in sorted population after vehicle treatment

Gene Name	Gamma	-log(p-val)	Notes
TRIM46	5.88	1.45	E3 ubiquitin ligase; neuronal
UBD	5.49	1.83	Ubiquitin D
TAPT1	5.37	1.51	
OSBPL5	3.75	1.95	
SCAMP2	3.56	1.52	
DNAJA2	3.50	1.59	
BPIFB4	3.49	1.71	
CRYAA	3.45	1.76	
MGAT2	3.34	1.39	
NOSIP	3.21	2.26	E3 ubiquitin ligase; neuronal
NELFA	3.13	1.34	

Gene Name	Gamma	-log(p-val)	Notes
HNRNPC	3.02	2.04	
CCDC115	3.01	1.46	
ECE2	2.95	1.70	
DYNC1LI2	2.95	1.56	
OSTM1	2.93	1.56	E3 ubiquitin ligase
ANKRD13A	2.80	1.83	
PDCL	2.64	1.46	
TBCA	2.48	1.42	
CHIP	2.41	1.39	E3 ubiquitin ligase; LRRK2-associated
ADAMTS10	1.99	1.38	
NPAS4	1.86	1.54	
RNF111	1.83	2.18	E3 ubiquitin ligase
PYDC1	1.71	1.39	
FBXW5	1.68	1.31	Substrate recognition component of E3 ligase complex
KBTBD2	1.63	1.40	
PHF7	1.55	1.69	
CTRC	1.50	2.23	
CNOT1	1.49	1.73	
DNAJB12	1.48	1.51	
RPL6	1.46	1.72	
FUNDC1	1.41	1.42	
ATP9B	1.39	1.80	
FBXO21	1.37	1.77	Substrate recognition component of E3 ligase complex
TTC7B	1.34	1.67	
KRT78	1.33	1.54	
SVIP	1.29	1.79	
ARL6IP1	1.27	1.57	
C5orf15	1.27	1.83	
RPL7A	1.27	1.69	
LPCAT3	1.26	1.32	
HSPA12B	1.25	1.53	
SLC13A5	1.25	1.31	
TMEM63C	1.18	2.08	
RAB1A	1.18	2.15	
GPR26	1.16	1.85	
GLCE	1.15	1.45	
CPA5	1.14	1.32	
PDIA3	1.13	1.71	
LRSAM1	1.12	1.45	E3 ubiquitin ligase
TSTD1	1.11	1.32	

Gene Name	Gamma	-log(p-val)	Notes
TMEM39A	1.08	2.03	
RPL36AL	1.07	2.35	
PSMD10	1.04	1.47	Proteasomal assembly protein
DNAJC5B	1.02	1.51	
SCAMP5	1.00	1.59	
C19orf52	1.00	2.08	
RPL12	1.00	1.65	
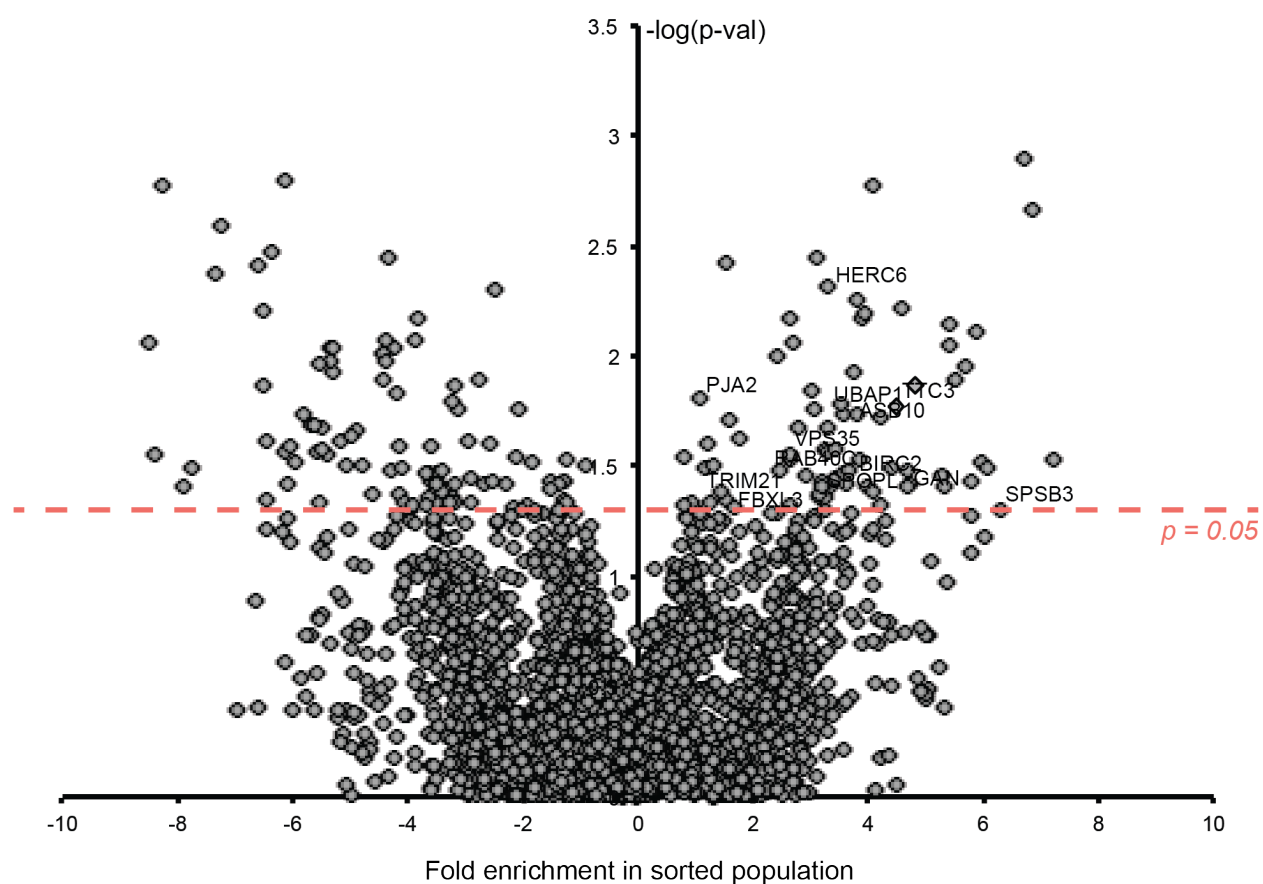
Figure 4.6. Genes involved in kinase inhibitor-dependent LRRK2 turnover. Volcano plot of 3,093 stress and proteostasis genes showing negative log of p-values vs. their sgRNA enrichment in sorted population relative to unsorted population for MLi-2-treated cells (tau). Significance is defined as $p < 0.05$, indicated by the red dashed line. Notable genes are labeled (see Table 4.2 for details).

Table 4.2. Enriched genes in sorted population after LRRK2 kinase inhibition

Gene Name	Tau	-log(p-val)	Notes
TSPAN8	7.21	1.53	
NKTR	6.85	2.67	
HNRNPK	6.72	2.90	
SPSB3	6.30	1.31	Substrate recognition component of E3 ligase complex
NFE2L3	6.05	1.49	
CRYBA1	5.99	1.52	
SPATA5	5.86	2.11	
RNF215	5.79	1.44	
DNAJC12	5.68	1.96	
YIPF3	5.49	1.90	
RANBP10	5.43	2.05	
OTX2	5.41	2.14	
HIST1H2BE	5.34	1.41	
SEC63	5.28	1.46	
PSMF1	4.84	1.87	
GAN	4.73	1.43	Substrate-specific adapter of E3 ligase complex; neuronal
NEUROG2	4.69	1.48	
PM20D2	4.68	1.41	
MEOX1	4.59	2.22	
TTC3	4.47	1.77	E3 ubiquitin ligase
DNAJA3	4.39	1.49	
OTX1	4.22	1.72	
CFI	4.21	1.32	
CNPY3	4.08	2.77	
LYPLA2	4.06	1.38	
RPH3A	3.96	1.40	
GALNT15	3.95	2.19	
SLC35A4	3.89	2.17	
TMEM168	3.83	1.54	
ASB10	3.81	1.74	Substrate recognition component of E3 ligase complex
LRRC48	3.80	2.26	
GORASP2	3.76	1.93	
PRPF3	3.66	1.48	
BIRC2	3.63	1.42	E3 ubiquitin ligase
GMPPB	3.56	1.47	
UBAP1	3.56	1.74	Ubiquitin binding protein
DR1	3.50	1.79	
ATP5I	3.45	1.45	
FAP	3.43	1.58	

Gene Name	Tau	-log(p-val)	Notes
SPOPL	3.34	1.41	E3 ligase complex component
ADAMTS1	3.30	1.57	
SLC2A8	3.29	1.67	
HERC6	3.27	2.32	E3 ubiquitin ligase
ATP5L	3.25	1.42	
WDR25	3.25	1.57	
ACTR1A	3.24	1.36	
LBP	3.21	1.41	
C10orf32	3.18	1.43	
VPS13A	3.17	1.36	
GALNT2	3.16	1.37	
SSR2	3.11	2.45	
UNC13D	3.06	1.76	
TMPRSS6	3.01	1.84	
EIF4A1	2.93	1.46	
ISL1	2.77	1.67	
ATG4B	2.69	2.06	
RP2	2.66	1.52	
GIMAP1	2.65	1.32	
ZNFX1	2.65	2.17	
VPS35	2.63	1.55	PD gene
RAB40C	2.45	1.48	Substrate recognition component of E3 ligase complex
ARRDC2	2.41	2.00	
ADAM7	1.79	1.62	
FBXL3	1.69	1.31	Substrate recognition component of E3 ligase complex
NEU4	1.57	1.72	
TTC9	1.54	1.34	
HES1	1.53	2.43	
NKX2-2	1.46	1.39	
EIF5B	1.32	1.50	
TRIM21	1.24	1.34	E3 ubiquitin ligase
DYNC1I1	1.20	1.61	
SCRN3	1.17	1.50	
PJA2	1.08	1.80	E3 ubiquitin ligase

PJA2 and BIRC2 cause LRRK2 degradation downstream of kinase inhibition

Of the 76 significantly enriched genes in the MLi-2 treated sorted sample, we chose to focus first on the E3 ubiquitin ligases. Five E3 ligases were found with tau > 1: BIRC2, HERC6, PJA2, TRIM21, and TTC3. We followed up with these hits by knocking down each target independently with 2-4 pooled sgRNAs in our dox-inducible GFP-LRRK2/dCas9 cells. While some of the E3 ligase hits from the screen did not validate individually, we consistently saw that knocking down either PJA2 or BIRC2 led to decreased LRRK2 turnover following kinase inhibition. We stably knocked down BIRC2 and PJA2 (7.0% +/- 2.2% and 6.6% +/- 1.4% relative mRNA expression, respectively) (Figure 4.7A) and measured LRRK2 turnover over time after dox-induction at 2 ng/mL. After 16 hours of MLi-2 treatment, both lines with targeted E3 ligases knocked down had turned over approximately 8% of their baseline GFP-LRRK2 (relative to cells not treated with MLi-2), compared to 30% in cells with a control sgRNA (Figure 4.7B). After 24 hours of inhibition, cells with control sgRNA had turned over 58.3% +/- 2.8% of their total LRRK2 relative to cells not treated with MLi-2. At the same time point, cells with PJA2 knocked down had turned over 47.3% +/- 3.4% of GFP-LRRK2, and cells with BIRC2 knocked down had turned over just 24.9% +/- 4.1% of GFP-LRRK2 (Figure 4.7B). These data indicate that loss of either PJA2 and especially BIRC2 significantly impacts the rate of LRRK2 turnover following kinase inhibition.
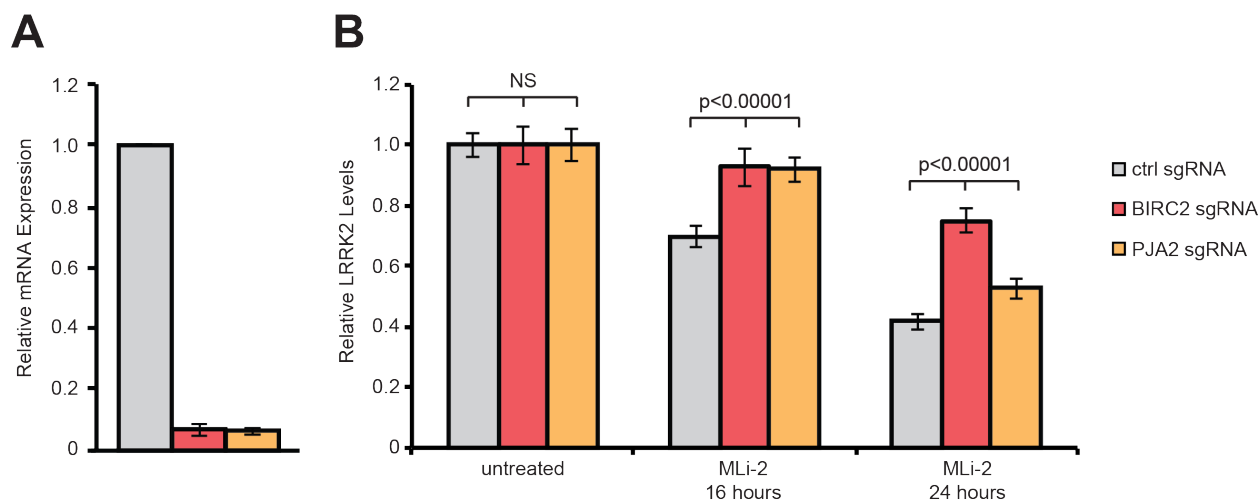
Figure 4.7. Knockdown of BIRC2 and PJA2 decrease LRRK2 kinase inhibition-driven turnover. (A) Relative BIRC2 and PJA2 mRNA expression in dox-inducible GFP-LRRK2 HEK-293T cells with dCas9 and either non-targeting sgRNA (grey bar), four pooled BIRC2-targeting sgRNAs (red bar), or two pooled PJA2-targeting sgRNAs (orange bar). (B) Flow cytometric quantification of GFP-LRRK2 levels with BIRC2 (red) or PJA2 (orange) knockdown and control line (grey) without kinase inhibition or after 16 or 24 hours of MLi-2 treatment (100 nM).

Discussion

LRRK2 kinase inhibition is a promising therapeutic strategy for PD; however, deleterious effects in peripheral organs, such as the accumulation of lamellar bodies in the lungs, present a challenge for the safe use of these drugs. The relationship between LRRK2's kinase activity and protein levels is not well understood, but may be important for finding an effective and safe therapy. To that end, we identified two new LRRK2-associated E3 ligases – BIRC2 and PJA2 – that appear to be important for regulating LRRK2 turnover specifically in the context of LRRK2 kinase inhibition. While it is known that kinase inhibitors cause LRRK2 to be ubiquitinated and degraded, we found that none of the known LRRK2-associated E3 ligases appear to be involved in that process. This fits broadly with the results of our CRISPRi screen, which found minimal

overlap in knocked down genes that led to increased LRRK2 levels with MLi-2 treatment and those that led to increased levels with vehicle treatment. This suggests that LRRK2 turnover is regulated differently under normal conditions versus with pharmacological intervention.

This preliminary work is just a starting point for understanding the effect of BIRC2 and PJA2 on LRRK2 turnover. We would first like to validate these findings with endogenous LRRK2. We would also like to look at LRRK2 turnover after kinase inhibition with both proteins knocked out in the same cell line to see if we can completely block LRRK2 degradation. If we are able to maintain protein levels while inhibiting LRRK2 kinase activity through a knockout, we could additionally look at readouts of LRRK2 neuronal toxicity (e.g. neurite outgrowth) and peripheral organ health (e.g. lung pathology). If we are successfully able to separate LRRK2 turnover from LRRK2 kinase inhibition, we may be able to understand more fully if LRRK2 toxicity is tied to LRRK2 kinase activity or protein levels, as well as determine whether LRRK's kinase-independent functions are essential for PD-related phenotypes and/or lung and kidney health.

Beyond following up on BIRC2 and PJA2, there are a lot of other data to mine from this turnover regulation CRISPRi screen. First, we would like to repeat the screen from the point of infecting cells with the sgRNA library to get more statistical strength. We already identified what may be false positive hits (i.e. HERC6, TRIM21, and TTC3 did not validate as E3 ligases important for LRRK2 turnover with inhibition), and it is possible that there are true hits that were missed, as well. This is not surprising given that we screened over 3,000 genes and used a cutoff of $p < 0.05$, but replication should help identify important hits amid the statistical noise. Furthermore, there are a number of non-E3 ligase enriched genes that may be worth pursuing in both the MLi-2 treated data set and the vehicle-treated set. Of particular interest are Rab1A, a

Rab protein that is also a LRRK2 substrate [39, 103], which was significant in the vehicle-treated population; Gigaxonin (GAN), which is an E3 ubiquitin ligase complex component and is important in neuronal maintenance and architecture [104]; and VPS35, a component of the retromer complex that is linked to autosomal dominant typical-onset PD, just like LRRK2. Finally, we have only examined here the enriched sgRNAs in the top LRRK2-expressing cells. We could also examine which genes had significantly depleted sgRNA counts or repeat the screen to sort for low LRRK2-expressing cells to identify targets important for stabilizing LRRK2 and preventing turnover.

CHAPTER V: CONCLUSIONS

PD is a major health challenge, affecting nearly 1 million Americans [1]. There are currently no treatments that prevent, slow, or reverse the course of the disease. While most cases of PD are idiopathic, a segment of cases are familial, and this discovery has led to new hope for understanding and treating PD. The majority of single-gene mutations that lead to PD cause atypical, early onset disease; however, mutations in LRRK2 lead to typical onset PD that is indistinguishable from idiopathic disease. LRRK2 mutations in familial and sporadic cases of PD account for the largest fraction of disease cases with a known cause. Thus, understanding LRRK2 biology may lead to a greater understanding of PD pathogenesis in general. Unfortunately, LRRK2 has been a challenging protein to investigate as it is large and complex, with two distinct enzymatic domains (GTPase and kinase) and multiple large protein-protein interaction domains. Recent proteomic approaches have had great success in identifying novel LRRK2 interactors and substrates [39, 60]. These approaches have led to new hypotheses on the role of LRRK2 in cells and in disease.

Here, we used two screening systems – an AP-MS proteomic screen and a CRISPRi genetic screen – to identify new proteins important for LRRK2 regulation. In our proteomic screen, we used full-length LRRK2, while previous studies have used truncated forms of LRRK2 for ease of expression. We hypothesized that focusing on the catalytic core and leaving off the N-terminus of LRRK2 would miss important interactors, and our results supported that idea. We identified TRIM1 as a novel interactor, and found that it binds an N-terminal region of LRRK2 between the Ankyrin and LRR domains – a region of the protein than previous MS screens have left out. In addition to TRIM1, our screen identified dozens of other novel interactors that may

be worth following up on to understand LRRK2 biology. Our second screen utilized CRISPRi with a novel flow cytometry assay to identify modifiers of LRRK2 turnover. The development of this flow cytometric assay allowed us to interrogate LRRK2 expression on a cell-by-cell basis, and selectively sort subpopulations for downstream analysis, compared to relying on assessing individual candidate proteins previously. Together, these two screens were successful in identifying novel LRRK2-associated proteins and furthering our understanding of LRRK2 regulation.

Our findings centered on two important components of LRRK2 biology: localization and protein degradation. We found that TRIM1 expression has a striking effect on LRRK2 localization along microtubules. No other interactor has been found to have such a profound ability to regulate LRRK2 localization. We would still like to verify this colocalization on an endogenous level, but unfortunately, we have not yet been able to find or develop the tools necessary to do so. We observed that LRRK2 co-localized with TRIM1 gives the appearance of discrete punctae, suggesting the presence of protein complexes. Identifying additional components of the TRIM1/LRRK2 complex, potentially through a narrower MS screen, may be useful for further understanding the role LRRK2 plays at the microtubule. Microtubules have long been of interest in PD and LRRK2 biology: they are important for neurite architecture, vesicular trafficking, mitophagy, and a number of other cellular processes that are disrupted in PD. Furthermore, dopaminergic neurons are especially sensitive to microtubule stability [56], so a link between LRRK2 biology and microtubules could in part explain the cell type specificity of PD when LRRK2 is expressed throughout the body.

We also found that TRIM1 ubiquitinates LRRK2 and targets it for proteasomal degradation. LRRK2 turnover is an important process – over-abundance of LRRK2 protein, WT

or mutant, can cause cytotoxicity [50]. Dysregulation of LRRK2 protein levels through impaired degradation may also be a common mechanism through which various mutations in LRRK2 lead to familial and idiopathic forms of PD. Furthermore, proteasomal degradation is especially important in the context of mutant LRRK2, which is not degraded efficiently via autophagy, and thus requires a greater proportion of protein to be turned over by the proteasome in order to maintain homeostasis [51]. Despite the importance of LRRK2 turnover, TRIM1 is just the fourth E3 ubiquitin ligase associated with LRRK2, and the second that causes LRRK2 degradation via the proteasome.

Interestingly, we found that regulation of LRRK2 turnover, localization, and kinase activity are connected via TRIM1 versus 14-3-3 binding on the LRRK2 Regulatory Loop. This region on LRRK2 is phosphorylated by unknown upstream kinases, leading to LRRK2 activation. Rab29, a LRRK2 regulator, enhances this process [43]. However, TRIM1 inhibits Rab29-mediated activation, and preferentially binds dephosphorylated LRRK2, targeting it for degradation. We also see that TRIM1 rescues LRRK2 G2019S-mediated cytotoxicity in the form of neurite outgrowth defects. For the inhibition of Rab29-mediated activation, we find that TRIM1's E3 ligase function, but not its microtubule localization, is critical; however, we don't yet know if the same is true for remediation of the LRRK2 G2019S phenotype. These data suggest that LRRK2 turnover is an effective strategy for combatting excessive LRRK2 kinase activity, but also underscore the open questions around the relationship among LRRK2 activity, localization, and stability. Going forward, we could utilize TRIM1 mutants (TRIM1ΔRF, cytoplasmic TRIM1, and B-Box mutant TRIM1 that cannot bind LRRK2) to further interrogate the interplay between these functions.

Because LRRK2 kinase inhibitors increase LRRK2's microtubule association and cause LRRK2 ubiquitination and degradation [42], we initially hypothesized that TRIM1 may be a critical regulator of LRRK2 turnover downstream of kinase inhibition. However, we found that loss of TRIM1 expression had no effect on LRRK2 turnover after treatment with small molecule inhibitors. Instead, we identified two additional E3 ligases that have not previously been linked to LRRK2: BIRC2 and PJA2 (however, notably, PJA2 was also a novel hit in our LRRK2 interactome that we did not initially pursue). Investigations into these new regulators are still in their early stages. Ultimately, we would like to understand if these E3 ligases are essential for LRRK2 degradation following kinase inhibition, and if so, what role LRRK2 protein levels play in neuronal health and lung/kidney homeostasis beyond the presence or absence of LRRK2 kinase activity. Furthermore, it could be useful to better understand the tissue-level specificity of LRRK2 turnover. A similar CRISPRi screen could be done in various cell types to determine if modifiers of LRRK2 levels are consistent or variable. This may also help us understand other LRRK2-associated diseases, like Crohn's disease and leprosy, which may be linked to LRRK2 degradation in immune cells. Beyond leading to a better understanding of LRRK2 biology, it is possible that targeting LRRK2 protein levels, either alongside or instead of targeting kinase activity, may be a useful therapeutic strategy in PD.

CHAPTER VI: MATERIALS AND METHODS

Cell lines and tissue culture

All cell lines were grown at 37°C in a humidified atmosphere with 5% CO_2. Human HEK-293T cells were cultured in DMEM with 10% FBS. Doxycycline-inducible GFP-LRRK2 HEK-293T cell lines, including those with dCas9, were cultured in DMEM with 10% tetracycline-free FBS, 10 μg/mL blasticidin, and 100 μg/mL hygromycin. Human H1299 cells were cultured in RPMI media with 10% FBS, 25 mM Hepes, and 2.0 g/L $NaHCO_3$. Doxycycline-inducible LRRK2 rat PC-12 cell lines [87] were grown in DMEM supplemented with 10% horse serum, 5% tetracycline-free FBS, 2 mM glutamax, 100 U/mL penicillin G, 100 μg/mL streptomycin, 400 μg/mL G418, and 200 μg/mL hygromycin and were differentiated under low-serum conditions the same media containing 1% horse serum without FBS and 100 ng/mL NGF. Mouse BV2 cells were cultured in RPMI media with 10% FBS and 2 mM glutamax. Human SH-SY5Y cells were cultured in 50% DMEM/50% F12 media with 10% FBS. Human SK-N-SH cells were cultured in DMEM with 10% FBS. Human A549 cells were cultured in F-12K media with 10% FBS.

Transfection and drug treatment

HEK-293T cells were transfected using Fugene 6 or Lipofectamine LTX generally, or Mirus for lentiviral library production; H1299 cells were transfected with Lipofectamine 2000; and PC12 cells were transfected with Lipofectamine LTX or Lipofectamine 3000, all per manufacturer's instructions. LRRK2 expression was induced with 2 ng/mL to 1 μg/mL doxycycline. The proteasomal inhibitor MG132 was used at 2 μM for 24 hours. Autophagy was

inhibited with chloroquine at 25 µM for 24 hours. MLi-2 was used at 100 nM to 10 µM for 24 to

48 hours. All other LRRK2 inhibitors were used at 10 µM for 24 hours.

Plasmids

Plasmids pcDNA5 frt/to expressing GFP-tagged human LRRK2, both full-length and

mutants and pCMV-C2-6myc or pCMV-C2-EGFP expressing WT human TRIM18 and TRIM1,

both full-length and domain mutants have been previously described [42, 105] as has plasmid

V5-14-3-3 theta [55]. Plasmid expressing mCherry-tubulin was a gift from Roger Tsien [106],

and plasmid pRK5-HA-ubiquitin WT was a gift from Ted Dawson (Addgene plasmid #17608)

[107].

Full-length human LRRK2 with N-terminal myc and FLAG tags was cloned into

pcDNA5 frt/to. In brief, pCMV-2myc-LRRK2, a gift from Mark Cookson (Addgene plasmid

#25361) [108] was cloned into pcDNA5 frt/to by site-directed mutagenic removal of a single

LRRK2 internal HpaI site (Quikchange, Stratagene), followed by HpaI/Eco53KI digest, ligation

into EcoRV site, and return of HpaI site. A 2x FLAG tag was introduced upstream of the 2x

myc tag by quikchange. Addgene plasmid #25361 was found to have the Arg50His variant not

present in consensus Uniprot sequence (Q5S007) and site-directed mutagenesis was used to

create Arg50.

Plasmid expressing GFP-LRRK2$_{822-982}$ was created by introducing a stop codon in GFP-

LRRK2$_{822-2527}$. Western blot was used to verify that there was no read-through of the stop

codon.   Plasmid expressing mCherry-myc-TRIM1 was created by cloning myc-TRIM1 into

pmCherry-C1 (Clontech). Plasmid expressing EBFP-14-3-3 was created using HiFi Cloning

(NEB). A CHIP plasmid [109] was a gift from Leonard Petrucelli and the CHIP ORF was cloned into pCMV-C2-6myc. All constructs were verified by DNA sequencing.

UCOE- EF1α-dCas9-BFP-KRAB used to generate CRISPRi lines was a gift from Martin Kampmann. The CRISPRi sgRNA parental plasmid was a gift from Jonathan Weissman (Addgene plasmid #84832) [110]. Individual sgRNA oligos were synthesized based on predicted sequences from supplementary file 3 in *Horlbeck et al.* [110] (see Table 6.1 below) and were cloned into the sgRNA parental plasmid and sequenced. Lentiviral plasmids dMD2.G and dR8.2 were gifts from Didier Trono (Addgene plasmids #12259 and #12263). The hCRISPRi-v2 subpooled stress/proteostasis library was a gift from Jonathan Weissman (Addgene #83973) [110].

Antibodies

The following antibodies were used: mouse anti-LRRK2 (Neuromab, N241A/34), rabbit anti-LRRK2 (MJFF c41-2), rabbit anti-phospho-Ser910 LRRK2 (Abcam, UDD 1 15(3)), rabbit anti-phospho-Ser935 LRRK2 (Abcam, UDD2 10(12)), rabbit anti-FLAG (Sigma, F7425), mouse anti-myc (Sigma, clone 9E10, M4439), rabbit anti-mCherry (Abcam, ab167453), rabbit anti-TRIM1 (Sigma, M2448), mouse anti-GFP (ThermoFisher, clone GF28R, MA5-15256), rabbit anti-HA (Cell Signaling, clone C29F4, 3724S), mouse anti-HA (Sigma, H7411), mouse anti-V5 (ThermoFisher, clone E 10/V4RR, MA5-15253), and mouse anti-actin (Sigma, A1978). For western blot, all primary antibodies were used at 1:500-1000 dilution except actin (1:1000-1:5000) and secondary antibodies (IRDye® 800CW or 680RD Goat anti-Mouse or anti-Rabbit IgG, LI-COR) were utilized at 1:10,000 dilution.

For immunoprecipitation and co-immunoprecipitation, the following pre-conjugated agarose-resin systems were used according to manufacturer instructions: anti-FLAG M2 (Sigma, A2220); GFP-trap®_A, myc-trap®_A, or mCherry-trap®_A (Chromotek); Pierce anti-HA (Thermo), and magnetic anti-V5 beads (MBL International).

Immunoprecipitation, mass spectrometry, and data analysis of LRRK2 interactome

Following transfection of HEK-293T cells, FLAG affinity purification followed by mass spectrometry was carried out as described in *Jager et al.* [72] except that elution of bound proteins was done using 100 mg/mL FLAG peptide (Sigma, F3290). Protein samples were subsequently reduced and alkylated, and digested with trypsin overnight at 37°C. Peptides were then desalted on C18 ziptip columns, lyophilized to dryness, and resuspended in 0.1% formic acid for injection into a Thermo Scientific LTQ Orbitrap XL Mass Spectrometer. For AP-MS experiments, raw data conversion and Protein Prospector search were also performed as described previously [72].

Co-immunoprecipitation

Cells were lysed in M-PER buffer or immunoprecipitation buffer (50 mM Tris pH 7.5, 150 mM NaCl, 1 mM EDTA, and 0.5% NP-40) supplemented with cOmplete protease inhibitor and Phostop phosphatase inhibitor. Cells were lysed by pipetting up and down and cell lysates were rotated at 4°C for 30 min then debris pelleted at 10,000 rpm for 5 min. 15-60 µL antibody-conjugated beads (GFP, FLAG, HA, or myc) were added and immunoprecipitations were performed at 4°C for 1-12 hours. Beads were washed at least 3 times in wash buffer (50 mM Tris pH 7.5, 500 mM NaCl, 1 mM EDTA) and bound proteins eluted by boiling in 40-100 µL 4x SDS

loading dye. All imaging and quantification of immunoblots was performed using a LI-COR

Odyssey® CLx imaging system.

Live cell microscopy

Spinning disk confocal live cell imaging was performed under environmentally

controlled conditions, essentially as described in *Stebhens et al.* [111] except that the system was

upgraded with a next generation scientific CCD camera (cMyo, 293 Photometrics) with 4.5 um

pixels allowing optimal spatial sampling using a 60x NA 1.49 objective (CFI 294 APO TIRF;

Nikon).

Flow Cytometry

GFP-LRRK2 levels were measured in doxycycline-inducible cell lines on a Fortessa flow

cytometer (BD Biosciences). Cells were induced with 2-5 ng/mL doxycycline, and doxycycline

was washed from cells 18-72 hours prior to analysis. GFP intensity was measured using a 488

nm laser for excitation, and a detector with a 505-nm long pass filter and a 525/50-nm band pass

filter. BFP intensity, where applicable, was measured using a 405 nm laser for excitation, and a

detector with a 450/50-nm band pass filter. Only live, single cells, as determined by forward and

side scatter, were analyzed.

CRISPRi knockdown

Catalytically dead Cas9 (dCas9-BFP) was inserted randomly into doxycycline-inducible

GFP-LRRK2 HEK-293T cells via lentiviral transduction. Cells were sorted for a BFP+ pure

population. Top predicted sgRNA sequences based on *Horlbeck et al.* [110] (Table 6.1) were

cloned into the parental sgRNA backbone. Lentivirus particles were made by transfecting dMD2.G, dR8.91, and sgRNA plasmids (1:9:10 ratio) into HEK-293T cells with lipofectamine 2000. Virus was harvested from media 72 hours after transfection and concentrated with LentiX concentrator (Takara Bio) per the product instructions. Cells were transduced, and then puromycin-selected (0.75 µg/mL) for 2 days before cells were plated and induced for included experiments. Knockdown was measured via real-time quantitative PCR (Table 6.2) with a non-targeting guide RNA used as a control.

Table 6.1. sgRNA sequences

sgRNA ID	Sequence
OR2AT4 (control)	CCAAGGTAGCATTGGTCTGT
TRIM1 sg1	GGGGCAGCACCATGACACCA
TRIM1 sg2	GCTCCGGTCACTCCTGCCAG
TRIM1 sg3	GCCCCCAGCCCTTCCTCTGG
TRIM1 sg4	GCATGTAAACGTGCCTCCAG
CHIP sg1	GGCCGGGTGCCGGAGAACGA
CHIP sg2	GGGCGGAACCCCAGGTGGTC
WSB1 sg1	GGGCGGCGCCGGAGATATCT
WSB1 sg2	GCCGACTGCAAACGAGACAC
BIRC2 sg1	GCCGCAGAGCCGGGAATCAG
BIRC2 sg2	GCGGCGCCGACAAGGAGATA
BIRC2 sg3	GGTCAGAGTGAGCCCGGATG
BIRC2 sg4	GGCGGGCCGTATCTCCTTGT
HERC6 sg1	GCGTGCGGAGACAACAGCAG
HERC6 sg2	GACCACAGGGTCCTCTCGTG
HERC6 sg3	GGAGCTGCCAGGTGAGCGGG
HERC6 sg4	GGAATCCGGAGCAGGCGACA
PJA2 sg1	GGCCGCTGCACATTTCGGTG
PJA2 sg2	GGAGTTGGAGGCGGAGAAGA
TRIM21 sg1	GGGTTCACTCACCTTTACAG
TRIM21 sg2	GAGCGTTGAGTCCCCTGTAA
TTC3 sg1	GACCCGCTCCCTCCCGCCGT
TTC3 sg2	GGGCCCTCCACGTCAGCCGA
TTC3 sg3	GACGTCAGCCGACGGCGGGA

sgRNA ID	Sequence
TTC3 sg4	GAAGGGGCACCAGACCAAGG
TRAF6 sg1	GTGACCGCTGGGAAGCGAGG
TRAF6 sg2	GGCCTCCCCGCGCACTAGAA
TRAF6 sg3	GAGGTGGCGAAGGCTCCCAC
TRAF6 sg4	GCGGCAAACTCTGGATCCAG
PSMC4 sg1	GGAGGAGATAGGCATCTTGG
PSMC4 sg2	GAGCGGTGACAGATCATCCC
PSMC4 sg3	GTGGTCACTATGGAGGAGAT
PSMC4 sg4	GGAGGCCGGCTTGGTCACTA

Table 6.2. qPCR primers

Target	Forward Primer	Reverse Primer
Actin	AGAGCTACGAGCTGCCTGAC	AGCACTGTGTTGGCGTACAG
TRIM1	ATTGACCTGTCCAATCTGCCT	GTTCAGCGAGATAACATACCTGC
CHIP	AGCAGGGCAATCGTCTGTTC	CAAGGCCCGGTTGGTGTAATA
WSB1	GATGGAATTTGGAATGGTGAGGTT	CTTCCGTCATGTGTCCCAGC
PSMC4	CCGCTGGTCATCGGACAATTT	GCGCACATAATAGTTGGAGCCT
PJA2	CAGCAGCAATGGACCAAGAAT	TGCCTGTAATTGTCTGATACCCT
BIRC2	AGCACGATCTTGTCAGATTGG	GGCGGGGAAAGTTGAATATGTA
HERC6	ATTTGGAGACAATCGCTCTGG	TGCGAAACTAGGCCATCAATTC
TRAF6	TTGCCATGAAAAGATGCAGAGG	AGCCTGGGCCAACATTCTC
TTC3	GACCCTGAGGGAATCAAGGAT	GTGTGTAGGCCCTGTTTTCATAA

PC12 neurite outgrowth assay

Doxycycline-inducible LRRK2 G2019S PC12 cells were plated at 20,000 cells/well in 96-well plates and transfected with pmaxGFP at 30 ng/well (for analysis of cell morphology) and mCherry-TRIM1 or mCherry empty vector at 200 ng/well. 24 hours after transfection, cells were moved to poly-D-lysine coated cover slips (Neuvitro) in the presence and absence of 1 mg/mL doxycycline. 48 hours after transfection, media was changed to PC12 differentiation media +/- 1 mg/mL doxycycline. Cells were grown in differentiation media for 5 days with media changed every 48-60 hours. Cells were then fixed in 4% paraformaldehyde-PBS for 20 min, washed 3x with PBS, permeabilized in PBS with 10% goat serum, 0.4% Triton X-100, 30

mg/mL BSA and 10 mg/mL glycine for 1 hour, washed 3x with PBS, and mounted on slides using Vectashield hardmount with DAPI. All steps from fixation to mounting were performed at 25°C. Cells were imaged at 40X using a Keyence BZ-X700 fluorescence microscope; all cells containing both red and green fluorescence were imaged. The presence/absence of neurites was assessed using ImageJ. Dead cells were excluded from further analysis.

CRISPRi screen and analysis

Doxycycline-inducible GFP-LRRK2 with dCas9-BFP cells were plated so that at the time of infection, there would be at least 1,000 cells infected per sgRNA per treatment condition. 48 hours after plating, on "Day 0," cells were infected with lentiviral preparations of stress and proteostasis hCRISPRi-v2 subpooled library at a concentration with an expected infection rate of approximately 40%. Lentiviral supernatant was added with 8 µg/mL final concentration of polybrene. 24 hours after infection, on Day 1, cells were pooled and re-plated. On Day 2, cells were selected with 0.75 µg/mL puromycin. On Day 3, half of the cells (approximately 100 million) were pelleted and frozen in 10% DMSO/90% FBS as a baseline sample. The remaining cells were re-plated and re-selected with fresh puromycin. On Day 4, selection was removed and all plated cells were induced with 5 ng/mL doxycycline. 24 hours after induction, doxycycline was washed out and half of the plated cells were treated with 100 nM MLi-2 and the other half were treated with an equivalent volume of DMSO. 24 hours after treatment, all cells were harvested and counted. 50 million cells from each treatment (approximately 1,000-fold coverage of all sgRNAs) were pelleted and frozen as before as the unsorted reference population. The remaining cells were sorted on an Aria2 SORP. Live, single, sgRNA+ cells (as determined by

BFP fluorescence) were sorted by GFP signal. The top 10% of GFP-LRRK2 expressing cells from each treatment group were collected and frozen as described.

To prepare samples for sequencing, genomic DNA was extracted using a NucleoSpin Blood L kit (Macherey-Nagel). gDNA was size fractionated by digesting with restriction enzyme MfeI (New England BioLabs) overnight and fragments <1200 bp were purified to enrich for sgRNA-containing material. PCR was done to amplify sgRNA and add adapter sequences for Illumina sequencing. Additionally, each sample (i.e. inhibitor- vs. vehicle-treated, sorted vs. unsorted) was given a unique 6-nucleotide barcode at this stage. Finally, 270 bp PCR products were purified with SPRI bead selection (Beckman and Coulter). Pooled products were sequenced on an Illumina HiSeq4000 with a 10% phiX spike-in.

Statistical analysis

Images shown represent typical results of independent experiments repeated at least three times. ImageStudio software (LI-COR) was used to quantify immunoblots. Flow cytometry data was analyzed using FlowJo software (FlowJo LLC). Data represent the normalized median green fluorescence intensity and twice the standard error of the mean. General statistical analysis was performed with excel software. An unpaired, two-tailed Student's t-test was used to evaluate statistical significance. A p-value < 0.05 was considered statistically significant.

For the interactome, proteins were identified using Protein Prospector, and high-confidence protein-interactions were identified by label-free quantification of bait samples as compared to empty vector control using MSstats R-package [112]. Two separate experiments with two or three independent replicates of WT FLAG-LRRK2 compared to FLAG empty vector were included in the analysis. In the case of rare proteins in which peptides were seen in the

presence of LRRK2 but none were identified in the empty vector control, a Mann-Whitney U test was performed to identify proteins significantly increased in the LRRK2 sample.

For CRISPRi screen, raw sequencing files were matched to hCRISPRi-v2 sgRNA sequences and counted per each condition. Phenotype values were calculated based on the relative enrichment or depletion of detected sgRNAs for all genes in each sample. P values were determined for each gene by a Mann-Whitney U test. Analysis was done in Enthought Canopy with modified python scripts from https://github.com/mhorlbeck/ScreenProcessing [113].

REFERENCES

1.   Kang, U.B. and J.A. Marto, *Leucine-rich repeat kinase 2 and Parkinson's disease.* Proteomics, 2017. **17**(1-2).

2.   Greggio, E. and M.R. Cookson, *Leucine-rich repeat kinase 2 mutations and Parkinson's disease: three questions.* ASN Neuro, 2009. **1**(1).

3.   Marras, C., et al., *Prevalence of Parkinson's disease across North America.* NPJ Parkinsons Dis, 2018. **4**: p. 21.

4.   The Lewin Group, I., *Economic Burden and Future Impact of Parkinson's Disease.* 2019, Michael J. Fox Foundation for Parkinson's Research: New York.

5.   Dawson, T.M. and V.L. Dawson, *Molecular pathways of neurodegeneration in Parkinson's disease.* Science, 2003. **302**(5646): p. 819-22.

6.   Kalinderi, K., S. Bostantjopoulou, and L. Fidani, *The genetic background of Parkinson's disease: current progress and future prospects.* Acta Neurol Scand, 2016. **134**(5): p. 314-326.

7.   Dauer, W. and S. Przedborski, *Parkinson's disease: mechanisms and models.* Neuron, 2003. **39**(6): p. 889-909.

8.   George, J.L., et al., *Targeting the progression of Parkinson's disease.* Curr Neuropharmacol, 2009. **7**(1): p. 9-36.

9.   Kalia, L.V., S.K. Kalia, and A.E. Lang, *Disease-modifying strategies for Parkinson's disease.* Mov Disord, 2015. **30**(11): p. 1442-50.

10.   Del Rey, N.L., et al., *Advances in Parkinson's Disease: 200 Years Later.* Front Neuroanat, 2018. **12**: p. 113.

11.	Polymeropoulos, M.H., et al., *Mutation in the alpha-synuclein gene identified in families with Parkinson's disease.* Science, 1997. **276**(5321): p. 2045-7.

12.	Kitada, T., et al., *Mutations in the parkin gene cause autosomal recessive juvenile parkinsonism.* Nature, 1998. **392**(6676): p. 605-8.

13.	Valente, E.M., et al., *Hereditary early-onset Parkinson's disease caused by mutations in PINK1.* Science, 2004. **304**(5674): p. 1158-60.

14.	Cookson, M.R., *Parkinsonism due to mutations in PINK1, parkin, and DJ-1 and oxidative stress and mitochondrial pathways.* Cold Spring Harb Perspect Med, 2012. **2**(9): p. a009415.

15.	Bonifati, V., et al., *DJ-1(PARK7), a novel gene for autosomal recessive, early onset parkinsonism.* Neurol Sci, 2003. **24**(3): p. 159-60.

16.	Zimprich, A., et al., *Mutations in LRRK2 cause autosomal-dominant parkinsonism with pleomorphic pathology.* Neuron, 2004. **44**(4): p. 601-7.

17.	Paisan-Ruiz, C., et al., *Cloning of the gene containing mutations that cause PARK8-linked Parkinson's disease.* Neuron, 2004. **44**(4): p. 595-600.

18.	Vilarino-Guell, C., et al., *VPS35 mutations in Parkinson disease.* Am J Hum Genet, 2011. **89**(1): p. 162-7.

19.	Zimprich, A., et al., *A mutation in VPS35, encoding a subunit of the retromer complex, causes late-onset Parkinson disease.* Am J Hum Genet, 2011. **89**(1): p. 168-75.

20.	Kett, L.R. and W.T. Dauer, *Leucine-rich repeat kinase 2 for beginners: six key questions.* Cold Spring Harb Perspect Med, 2012. **2**(3): p. a009407.

21.	Gasser, T., *Usefulness of Genetic Testing in PD and PD Trials: A Balanced Review.* J Parkinsons Dis, 2015. **5**(2): p. 209-15.

22. Webber, P.J. and A.B. West, *LRRK2 in Parkinson's disease: function in cells and neurodegeneration.* Febs j, 2009. **276**(22): p. 6436-44.

23. Langston, R.G., I.N. Rudenko, and M.R. Cookson, *The function of orthologues of the human Parkinson's disease gene LRRK2 across species: implications for disease modelling in preclinical research.* Biochem J, 2016. **473**(3): p. 221-32.

24. Deng, J., et al., *Structure of the ROC domain from the Parkinson's disease-associated leucine-rich repeat kinase 2 reveals a dimeric GTPase.* Proc Natl Acad Sci U S A, 2008. **105**(5): p. 1499-504.

25. Di Fonzo, A., et al., *A common missense variant in the LRRK2 gene, Gly2385Arg, associated with Parkinson's disease risk in Taiwan.* Neurogenetics, 2006. **7**(3): p. 133-8.

26. Liu, Z., et al., *The kinase LRRK2 is a regulator of the transcription factor NFAT that modulates the severity of inflammatory bowel disease.* Nat Immunol, 2011. **12**(11): p. 1063-70.

27. Fava, V.M., et al., *A Missense LRRK2 Variant Is a Risk Factor for Excessive Inflammatory Responses in Leprosy.* PLoS Negl Trop Dis, 2016. **10**(2): p. e0004412.

28. Cookson, M.R., *The role of leucine-rich repeat kinase 2 (LRRK2) in Parkinson's disease.* Nat Rev Neurosci, 2010. **11**(12): p. 791-7.

29. Tong, Y., et al., *Loss of leucine-rich repeat kinase 2 causes impairment of protein degradation pathways, accumulation of alpha-synuclein, and apoptotic cell death in aged mice.* Proc Natl Acad Sci U S A, 2010. **107**(21): p. 9879-84.

30. Herzig, M.C., et al., *LRRK2 protein levels are determined by kinase function and are crucial for kidney and lung homeostasis in mice.* Hum Mol Genet, 2011. **20**(21): p. 4209-23.

31.   Chan, S.L. and E.K. Tan, *Targeting LRRK2 in Parkinson's disease: an update on recent developments.* Expert Opin Ther Targets, 2017. **21**(6): p. 601-610.

32.   Martin, I., et al., *LRRK2 pathobiology in Parkinson's disease.* J Neurochem, 2014. **131**(5): p. 554-65.

33.   Rudenko, I.N. and M.R. Cookson, *14-3-3 proteins are promising LRRK2 interactors.* Biochem J, 2010. **430**(3): p. e5-6.

34.   Dzamko, N., et al., *Inhibition of LRRK2 kinase activity leads to dephosphorylation of Ser(910)/Ser(935), disruption of 14-3-3 binding and altered cytoplasmic localization.* Biochem J, 2010. **430**(3): p. 405-13.

35.   Caesar, M., et al., *Leucine-rich repeat kinase 2 functionally interacts with microtubules and kinase-dependently modulates cell migration.* Neurobiol Dis, 2013. **54**: p. 280-8.

36.   Law, B.M., et al., *A direct interaction between leucine-rich repeat kinase 2 and specific beta-tubulin isoforms regulates tubulin acetylation.* J Biol Chem, 2014. **289**(2): p. 895-908.

37.   Bailey, R.M., et al., *LRRK2 phosphorylates novel tau epitopes and promotes tauopathy.* Acta Neuropathol, 2013. **126**(6): p. 809-27.

38.   Park, S., et al., *Interplay between Leucine-Rich Repeat Kinase 2 (LRRK2) and p62/SQSTM-1 in Selective Autophagy.* PLoS One, 2016. **11**(9): p. e0163029.

39.   Steger, M., et al., *Phosphoproteomics reveals that Parkinson's disease kinase LRRK2 regulates a subset of Rab GTPases.* Elife, 2016. **5**.

40.   Shi, M.M., C.H. Shi, and Y.M. Xu, *Rab GTPases: The Key Players in the Molecular Pathway of Parkinson's Disease.* Front Cell Neurosci, 2017. **11**: p. 81.

41. Sheng, Z., et al., *Ser1292 autophosphorylation is an indicator of LRRK2 kinase activity and contributes to the cellular effects of PD mutations.* Sci Transl Med, 2012. **4**(164): p. 164ra161.

42. Zhao, J., et al., *LRRK2 dephosphorylation increases its ubiquitination.* Biochem J, 2015. **469**(1): p. 107-20.

43. Purlyte, E., et al., *Rab29 activation of the Parkinson's disease-associated LRRK2 kinase.* Embo j, 2018. **37**(1): p. 1-18.

44. MacLeod, D., et al., *The familial Parkinsonism gene LRRK2 regulates neurite process morphology.* Neuron, 2006. **52**(4): p. 587-93.

45. Plowey, E.D., et al., *Role of autophagy in G2019S-LRRK2-associated neurite shortening in differentiated SH-SY5Y cells.* J Neurochem, 2008. **105**(3): p. 1048-56.

46. Heo, H.Y., K.S. Kim, and W. Seol, *Coordinate Regulation of Neurite Outgrowth by LRRK2 and Its Interactor, Rab5.* Exp Neurobiol, 2010. **19**(2): p. 97-105.

47. Liu, Z., et al., *A Drosophila model for LRRK2-linked parkinsonism.* Proc Natl Acad Sci U S A, 2008. **105**(7): p. 2693-8.

48. Imai, Y., et al., *The Parkinson's Disease-Associated Protein Kinase LRRK2 Modulates Notch Signaling through the Endosomal Pathway.* PLoS Genet, 2015. **11**(9): p. e1005503.

49. West, A.B., et al., *Parkinson's disease-associated mutations in leucine-rich repeat kinase 2 augment kinase activity.* Proc Natl Acad Sci U S A, 2005. **102**(46): p. 16842-7.

50. Skibinski, G., et al., *Mutant LRRK2 toxicity in neurons depends on LRRK2 levels and synuclein but not kinase activity or inclusion bodies.* J Neurosci, 2014. **34**(2): p. 418-33.

51.   Orenstein, S.J., et al., *Interplay of LRRK2 with chaperone-mediated autophagy.* Nat Neurosci, 2013. **16**(4): p. 394-406.

52.   Kikis, E.A., T. Gidalevitz, and R.I. Morimoto, *Protein homeostasis in models of aging and age-related conformational disease.* Adv Exp Med Biol, 2010. **694**: p. 138-59.

53.   Li, X., et al., *Phosphorylation-dependent 14-3-3 binding to LRRK2 is impaired by common mutations of familial Parkinson's disease.* PLoS One, 2011. **6**(3): p. e17153.

54.   Muda, K., et al., *Parkinson-related LRRK2 mutation R1441C/G/H impairs PKA phosphorylation of LRRK2 and disrupts its interaction with 14-3-3.* Proc Natl Acad Sci U S A, 2014. **111**(1): p. E34-43.

55.   Kett, L.R., et al., *LRRK2 Parkinson disease mutations enhance its microtubule association.* Hum Mol Genet, 2012. **21**(4): p. 890-9.

56.   Ren, Y., et al., *Selective vulnerability of dopaminergic neurons to microtubule depolymerization.* J Biol Chem, 2005. **280**(40): p. 34105-12.

57.   Marin, I., *The Parkinson disease gene LRRK2: evolutionary and structural insights.* Mol Biol Evol, 2006. **23**(12): p. 2423-33.

58.   Gilsbach, B.K. and A. Kortholt, *Structural biology of the LRRK2 GTPase and kinase domains: implications for regulation.* Front Mol Neurosci, 2014. **7**: p. 32.

59.   Baptista, M.A., et al., *Loss of leucine-rich repeat kinase 2 (LRRK2) in rats leads to progressive abnormal phenotypes in peripheral organs.* PLoS One, 2013. **8**(11): p. e80705.

60.   Beilina, A., et al., *Unbiased screen for interactors of leucine-rich repeat kinase 2 supports a common pathway for sporadic and familial Parkinson disease.* Proc Natl Acad Sci U S A, 2014. **111**(7): p. 2626-31.

61.   Nucifora, F.C., Jr., et al., *Ubiqutination via K27 and K29 chains signals aggregation and neuronal protection of LRRK2 by WSB1*. Nat Commun, 2016. **7**: p. 11792.

62.   Ding, X. and M.S. Goldberg, *Regulation of LRRK2 stability by the E3 ubiquitin ligase CHIP*. PLoS One, 2009. **4**(6): p. e5949.

63.   Nichols, R.J., et al., *14-3-3 binding to LRRK2 is disrupted by multiple Parkinson's disease-associated mutations and regulates cytoplasmic localization*. Biochem J, 2010. **430**(3): p. 393-404.

64.   Winner, B., et al., *Adult neurogenesis and neurite outgrowth are impaired in LRRK2 G2019S mice*. Neurobiol Dis, 2011. **41**(3): p. 706-16.

65.   Godena, V.K., et al., *Increasing microtubule acetylation rescues axonal transport and locomotor deficits caused by LRRK2 Roc-COR domain mutations*. Nat Commun, 2014. **5**: p. 5245.

66.   Melrose, H.L., et al., *Impaired dopaminergic neurotransmission and microtubule-associated protein tau alterations in human LRRK2 transgenic mice*. Neurobiol Dis, 2010. **40**(3): p. 503-17.

67.   Kawakami, F., et al., *LRRK2 phosphorylates tubulin-associated tau but not the free molecule: LRRK2-mediated regulation of the tau-tubulin association and neurite outgrowth*. PLoS One, 2012. **7**(1): p. e30834.

68.   Kawakami, F., et al., *Leucine-rich repeat kinase 2 regulates tau phosphorylation through direct activation of glycogen synthase kinase-3beta*. Febs j, 2014. **281**(1): p. 3-13.

69.   Short, K.M. and T.C. Cox, *Subclassification of the RBCC/TRIM superfamily reveals a novel motif necessary for microtubule binding*. J Biol Chem, 2006. **281**(13): p. 8970-80.

70.   Buchner, G., et al., *MID2, a homologue of the Opitz syndrome gene MID1: similarities in subcellular localization and differences in expression during development.* Hum Mol Genet, 1999. **8**(8): p. 1397-407.

71.   Geetha, T.S., et al., *Targeted deep resequencing identifies MID2 mutation for X-linked intellectual disability with varied disease severity in a large kindred from India.* Hum Mutat, 2014. **35**(1): p. 41-4.

72.   Jager, S., et al., *Global landscape of HIV-human protein complexes.* Nature, 2012. **481**(7381): p. 365-70.

73.   Collins, S.R., et al., *Toward a comprehensive atlas of the physical interactome of Saccharomyces cerevisiae.* Mol Cell Proteomics, 2007. **6**(3): p. 439-50.

74.   Swaney, D.L., et al., *Global analysis of phosphorylation and ubiquitylation cross-talk in protein degradation.* Nat Methods, 2013. **10**(7): p. 676-82.

75.   Ramage, H.R., et al., *A combined proteomics/genomics approach links hepatitis C virus infection with nonsense-mediated mRNA decay.* Mol Cell, 2015. **57**(2): p. 329-40.

76.   Perry, J., et al., *FXY2/MID2, a gene related to the X-linked Opitz syndrome gene FXY/MID1, maps to Xq22 and encodes a FNIII domain-containing protein that associates with microtubules.* Genomics, 1999. **62**(3): p. 385-94.

77.   Pankratz, N., et al., *Genome-wide linkage analysis and evidence of gene-by-gene interactions in a sample of 362 multiplex Parkinson disease families.* Hum Mol Genet, 2003. **12**(20): p. 2599-608.

78.   Sejwal, K., et al., *Cryo-EM analysis of homodimeric full-length LRRK2 and LRRK1 protein complexes.* Sci Rep, 2017. **7**(1): p. 8667.

79. Schmidt, S.H., et al., *The dynamic switch mechanism that leads to activation of LRRK2 is embedded in the DFGpsi motif in the kinase domain.* Proc Natl Acad Sci U S A, 2019. **116**(30): p. 14979-14988.

80. Thibaudeau, T.A., R.T. Anderson, and D.M. Smith, *A common mechanism of proteasome impairment by neurodegenerative disease-associated oligomers.* Nat Commun, 2018. **9**(1): p. 1097.

81. Kuzuhara, S., et al., *Lewy bodies are ubiquitinated. A light and electron microscopic immunocytochemical study.* Acta Neuropathol, 1988. **75**(4): p. 345-53.

82. Zhu, X., et al., *LRRK2 protein is a component of Lewy bodies.* Ann Neurol, 2006. **60**(5): p. 617-8; author reply 618-9.

83. Lobbestael, E., et al., *Identification of protein phosphatase 1 as a regulator of the LRRK2 phosphorylation cycle.* Biochem J, 2013. **456**(1): p. 119-28.

84. Ko, H.S., et al., *CHIP regulates leucine-rich repeat kinase-2 ubiquitination, degradation, and toxicity.* Proc Natl Acad Sci U S A, 2009. **106**(8): p. 2897-902.

85. Rudenko, I.N., et al., *The G2385R risk factor for Parkinson's disease enhances CHIP-dependent intracellular degradation of LRRK2.* Biochem J, 2017. **474**(9): p. 1547-1558.

86. Larson, M.H., et al., *CRISPR interference (CRISPRi) for sequence-specific control of gene expression.* Nat Protoc, 2013. **8**(11): p. 2180-96.

87. Migheli, R., et al., *LRRK2 affects vesicle trafficking, neurotransmitter extracellular level and membrane receptor localization.* PLoS One, 2013. **8**(10): p. e77198.

88. Das, K.P., T.M. Freudenrich, and W.R. Mundy, *Assessment of PC12 cell differentiation and neurite growth: a comparison of morphological and neurochemical measures.* Neurotoxicol Teratol, 2004. **26**(3): p. 397-406.

89.   West, A.B., *Ten years and counting: moving leucine-rich repeat kinase 2 inhibitors to the clinic.* Mov Disord, 2015. **30**(2): p. 180-9.

90.   West, A.B., *Achieving neuroprotection with LRRK2 kinase inhibitors in Parkinson disease.* Exp Neurol, 2017. **298**(Pt B): p. 236-245.

91.   Fell, M.J., et al., *MLi-2, a Potent, Selective, and Centrally Active Compound for Exploring the Therapeutic Potential and Safety of LRRK2 Kinase Inhibition.* J Pharmacol Exp Ther, 2015. **355**(3): p. 397-409.

92.   Fuji, R.N., et al., *Effect of selective LRRK2 kinase inhibition on nonhuman primate lung.* Sci Transl Med, 2015. **7**(273): p. 273ra15.

93.   Jones, L.H., *Small-Molecule Kinase Downregulators.* Cell Chem Biol, 2018. **25**(1): p. 30-35.

94.   Polier, S., et al., *ATP-competitive inhibitors block protein kinase recruitment to the Hsp90-Cdc37 system.* Nat Chem Biol, 2013. **9**(5): p. 307-12.

95.   Foulkes, D.M., et al., *Covalent inhibitors of EGFR family protein kinases induce degradation of human Tribbles 2 (TRIB2) pseudokinase in cancer cells.* Sci Signal, 2018. **11**(549).

96.   Burslem, G.M., et al., *The Advantages of Targeted Protein Degradation Over Inhibition: An RTK Case Study.* Cell Chem Biol, 2018. **25**(1): p. 67-77.e3.

97.   Dobrovolsky, D., et al., *Bruton tyrosine kinase degradation as a therapeutic strategy for cancer.* Blood, 2019. **133**(9): p. 952-961.

98.   Deng, X., et al., *Characterization of a selective inhibitor of the Parkinson's disease kinase LRRK2.* Nat Chem Biol, 2011. **7**(4): p. 203-5.

99.   Reith, A.D., et al., *GSK2578215A; a potent and highly selective 2-arylmethyloxy-5-substitutent-N-arylbenzamide LRRK2 kinase inhibitor.* Bioorg Med Chem Lett, 2012. **22**(17): p. 5625-9.

100.   Estrada, A.A., et al., *Discovery of highly potent, selective, and brain-penetrable leucine-rich repeat kinase 2 (LRRK2) small molecule inhibitors.* J Med Chem, 2012. **55**(22): p. 9416-33.

101.   Estrada, A.A. and Z.K. Sweeney, *Chemical Biology of Leucine-Rich Repeat Kinase 2 (LRRK2) Inhibitors.* J Med Chem, 2015. **58**(17): p. 6733-46.

102.   George, A.J., et al., *A Comprehensive Atlas of E3 Ubiquitin Ligase Mutations in Neurological Disorders.* Front Genet, 2018. **9**: p. 29.

103.   Jeong, G.R., et al., *Dysregulated phosphorylation of Rab GTPases by LRRK2 induces neurodegeneration.* Mol Neurodegener, 2018. **13**(1): p. 8.

104.   Opal, P. and R.D. Goldman, *Explaining intermediate filament accumulation in giant axonal neuropathy.* Rare Dis, 2013. **1**: p. e25378.

105.   Short, K.M., et al., *MID1 and MID2 homo- and heterodimerise to tether the rapamycin-sensitive PP2A regulatory subunit, alpha 4, to microtubules: implications for the clinical variability of X-linked Opitz GBBB syndrome and other developmental disorders.* BMC Cell Biol, 2002. **3**: p. 1.

106.   Shaner, N.C., et al., *Improved monomeric red, orange and yellow fluorescent proteins derived from Discosoma sp. red fluorescent protein.* Nat Biotechnol, 2004. **22**(12): p. 1567-72.

107.   Lim, K.L., et al., *Parkin mediates nonclassical, proteasomal-independent ubiquitination of synphilin-1: implications for Lewy body formation.* J Neurosci, 2005. **25**(8): p. 2002-9.

108. Greggio, E., et al., *The Parkinson disease-associated leucine-rich repeat kinase 2 (LRRK2) is a dimer that undergoes intramolecular autophosphorylation.* J Biol Chem, 2008. **283**(24): p. 16906-14.

109. Petrucelli, L., et al., *CHIP and Hsp70 regulate tau ubiquitination, degradation and aggregation.* Hum Mol Genet, 2004. **13**(7): p. 703-14.

110. Horlbeck, M.A., et al., *Compact and highly active next-generation libraries for CRISPR-mediated gene repression and activation.* Elife, 2016. **5**.

111. Stehbens, S.J., et al., *CLASPs link focal-adhesion-associated microtubule capture to localized exocytosis and adhesion site turnover.* Nat Cell Biol, 2014. **16**(6): p. 561-73.

112. Choi, M., et al., *MSstats: an R package for statistical analysis of quantitative mass spectrometry-based proteomic experiments.* Bioinformatics, 2014. **30**(17): p. 2524-6.

113. Gilbert, L.A., et al., *Genome-Scale CRISPR-Mediated Control of Gene Repression and Activation.* Cell, 2014. **159**(3): p. 647-61.

Publishing Agreement

It is the policy of the University to encourage open access and broad distribution of all theses, dissertations, and manuscripts. The Graduate Division will facilitate the distribution of UCSF theses, dissertations, and manuscripts to the UCSF Library for open access and distribution. UCSF will make such theses, dissertations, and manuscripts accessible to the public and will take reasonable steps to preserve these works in perpetuity.

I hereby grant the non-exclusive, perpetual right to The Regents of the University of California to reproduce, publicly display, distribute, preserve, and publish copies of my thesis, dissertation, or manuscript in any form or media, now existing or later derived, including access online for teaching, research, and public service purposes.

_____   1/28/2020
Author Signature   _____
                                                           Date